PREPARED FOR THE U.S. DEPARTMENT OF ENERGY,
UNDER CONTRACT DE-AC02-76CH03073

PPPL-3916
UC-70

PPPL-3916

Diverted Tokamak Carbon Screening: Scaling with Machine Size and Consequences to Core Contamination

by

J.D. Strachan, G. Corrigan, A.Kallenbach, G.F. Matthews, H. Meister,
R. Neu, V. Rohde, and J. Spence

January 2004

PPPL
PRINCETON PLASMA
PHYSICS LABORATORY

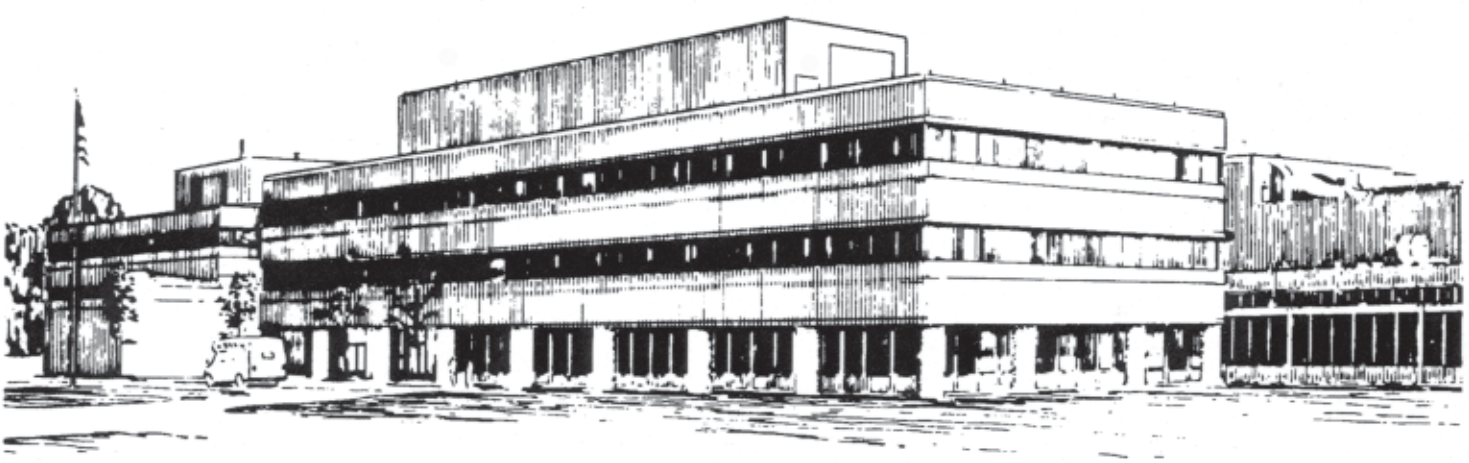

PRINCETON PLASMA PHYSICS LABORATORY
PRINCETON UNIVERSITY, PRINCETON, NEW JERSEY

PPPL Reports Disclaimer

Availability

This report is posted on the U.S. Department of Energy's Princeton Plasma Physics Laboratory Publications and Reports web site in Fiscal Year 2004. The home page for PPPL Reports and Publications is: http://www.pppl.gov/pub_report/

DOE and DOE Contractors can obtain copies of this report from:

U.S. Department of Energy
Office of Scientific and Technical Information
DOE Technical Information Services (DTIS)
P.O. Box 62
Oak Ridge, TN 37831

Telephone: (865) 576-8401

Fax: (865) 576-5728

Email: reports@adonis.osti.gov

This report is available to the general public from:

National Technical Information Service
U.S. Department of Commerce
5285 Port Royal Road
Springfield, VA 22161

Telephone: 1-800-553-6847 or
(703) 605-6000

Fax: (703) 321-8547

Internet: http://www.ntis.gov/ordering.htm

Diverted Tokamak Carbon Screening: Scaling with Machine Size and Consequences to Core Contamination

J. D. Strachan, G. Corrigan[1], A. Kallenbach[2], G. F. Matthews[1], H. Meister[2], R. Neu[2], V. Rohde[2], and J. Spence[1]

PPPL
Princeton University,
Princeton, NJ, 08543
USA

Jan. 22, 2004

[1] EURATOM/UKAEA, Culham Science Centre, Abingdon OX14 3DB, UK
[2] MPI fur Plasmaphysik, EURATOM-Assoziation, D-8046 Garching bei Munchen, Germany

Abstract:

Plasma impurity content depends upon the impurity sources, fuelling efficiency, and confinement. In JET, carbon is the primary impurity, and its fuelling efficiency has been studied using methane gas injection and modeled with the SOL codes: DIVIMP and EDGE2D. In this paper, EDGE2D modeling of similar AUG experiments and projections to ITER are described. The parameters have been identified which govern the size scaling of carbon screening.

Size scaling is complex. For carbon injected from the main chamber, the important factors include: the SOL temperature, the magnitude of the thermal force at the divertor entrance, and the parallel distance to the divertor. For carbon injected at the strike points, the intersection of the carbon ionization region with the region of strong thermal force determines the carbon fuelling efficiency

ITER projects to have much better carbon screening than JET. The ITER SOL is hotter so that main chamber carbon is ionized further from the separatrix making the calculated carbon fuelling efficiency lower. Also, the carbon originating near the strike point has less chance of escaping the divertor by factors of about 100. The carbon sputtering is projected to be larger by similar factors, making the projected ITER core contamination similar to JET. However, that result is based upon the assumption that the wall materials have similar composition and behavior as observed on JET. A general result is that the core contamination at fixed total sputtering rate and core impurity confinement increases when the fraction of carbon ionized in the main chamber SOL increases, and decreases for larger machine size and higher density operation.

INTRODUCTION:

The impurity contamination of a fusion reactor is a complex topic. Ideally, the contamination observed on existing experiments provides guidance about expected reactor contamination. Following that logic, this paper studies size scaling by extending modeling which fits JET experiments to other devices. The edge fluid/Monte-Carlo code, EDGE2D/NIMBUS [1], was used successfully to interpret JET carbon screening experiments [2]. Here, EDGE2D calculations of ASDEX UPGRADE (AUG) and ITER extended the JET results in order to see how the carbon behavior changes with different sized machines. The AUG calculations are benchmarked against an AUG screening experiment intended to directly test the size scaling.

Different machines have different dimensions, so we call the work a size scaling study. However, different devices can also have different density, power, and relative geometry of the plasma edge with the vessel. These other factors can also be important and are also the topic of this paper. The relevant similarity parameter for divertor operation is the SOL power divided by the major radius [3]. Since ITER has much higher power per major radius length, P/R, values than JET, direct simulations of ITER divertor conditions are difficult to perform on JET [3]. Consequently, the approach here is that recommended in [3] of validating models on JET and applying the models to ITER.

Simplistically, the impurity content is the product of three processes which each have their own scaling. In the order that this paper treats these processes, they are:

1) Screening is the ability of the impurity to penetrate to the core. This is a scrape-off-layer (SOL) process described here by EDGE2D. We consider the screening of both main chamber carbon (section IV), and divertor carbon (Section V). The screening is quantified by the carbon fuelling efficiency[1] defined as equation (1) of Ref. [2]. Good screening is indicated by a low carbon fuelling efficiency.
2) The impurity source (including recycling) rate (Section VI) is a wall or divertor target process, and may be different when different materials, conditioning techniques, or power densities are used. This process is difficult to scale between machines. In this paper,

[1] The carbon fuelling efficiency is called FE in this paper and was called S in Ref. [2].

the machine components are assumed similar to JET, keeping the experimental connection to the JET results.

3) The confinement of the impurity once in the core is a turbulent process that probably also determines the core particle and energy content. This process probably scales in a similar way to the core energy confinement. Here, we assume that the impurity transport is diffusive and described by a carbon diffusion coefficient, D_C. Other transport models are possible but have not been explored here.

Recently, an extensive experimental campaign documented JET carbon screening [2]. The results were modeled and interpreted with the DIVIMP [4] and EDGE2D [1] edge codes. A picture of the important screening processes was developed. This picture resulted in a semi-empirical model for the intrinsic impurity content in JET. The screening experiments, the numerical modeling, and the semi-empirical model described the JET intrinsic Z_{eff} and the inter-ELM carbon content rise using two toroidally symmetric intrinsic carbon sources ñ the main chamber and the divertor strike points. Therefore in this paper, we study separately, the size scaling of the carbon fuelling efficiency when carbon is injected from the horizontal mid-plane in the main chamber or from the vicinity of the outer strike point. Both locations are important impurity locations. The mid-plane is the region of poorest screening due to the thinness of the SOL at that region. The mid-plane screening results are then related to the screening integrated over the wall source. The outer strike point is the location of highest impurity generation.

In this paper, we extend the numerical modeling to derive a size scaling of the screening and sputtering rates to yield a scaling of the core contamination. The approach is to use JET calculations to identify the sensitive parameters aside from size. Keeping those parameters fixed, the AUG, JET, and ITER calculations are then used to derive the effects of machine size. There are several important size parameters such as the linear dimension of the divertor chamber, the parallel length to the divertor, the distance of the carbon ionization from the separatrix, and the toroidal length of the strike points. These lengths tend to be co-linear since they are all larger on larger devices, although the divertor size on JET is relatively smaller than on AUG or ITER. Our approach is to concentrate upon the plausibly important scale lengths for each process. For the screening of divertor sources, the size of the divertor chamber was considered important while for the magnitude of the impurity sources, the size of the divertor chamber and the strike point length were considered important. For main

chamber screening, the distance of carbon ionization from the separatrix is one important size parameter and another is the parallel distance to the divertor. For the core impurity confinement in a diffusive transport model, then the cross-sectional area of the core is the important size parameter.

The results indicate that larger machines screen carbon better than smaller machines. The basic phenomena are different for main chamber injected carbon than for divertor injected carbon. Main chamber injected carbon will be ionized further from the separatrix on ITER, than on AUG or JET, due to the higher expected SOL temperature, and the longer expected SOL temperature widths. Carbon injected at the outer strike point for the ITER simulation was also better screened than for AUG or JET due to the larger size of the divertor. The sputtering yields depend mostly upon the power flowing into the SOL, and so are larger for the larger machines.

The present study has a number of uncertainties (Section III) which are difficult to quantify. Probably the most important errors are the neglect of observed SOL flows, and the lack of ELM effects. Future work is being directed towards incorporating these processes.

This paper is organized into the following sections: Section II describes the ASDEX UPGRADE experimental results. Section III describes the EDGE2D modeling. Section IV describes the screening of carbon injected at the mid-plane. Section V describes the screening of carbon injected at the outer strike point. Section VI describes sputtered carbon rates assuming that the AUG and ITER machines were composed of the same material as JET. Section VII combines the results to predict the carbon content as a function of size.

II ASDEX UPGRADE EXPERIMENT

In order to benchmark the EDGE2D size scaling, a mid-plane methane injection experiment was performed on ASDEX UPGRADE (AUG) [5]. The goal of the experiment was to repeat the JET mid-plane screening experiments [2]. AUG 16300 was intended to replicate the JET L-Mode plasma 49705 (Table I). The AUG experiment was performed in hydrogen plasmas with CH_4 injection while the JET experiment was performed in deuterium plasmas with CD_4 injection. The hydrogen plasmas were used in order to obtain a higher H-Mode power threshold, making the L-Mode experiments viable, however, we assume that the isotope difference does not change the basic processes or their modeling. EDGE2D/NIMBUS does model each isotope. 49705 was the central case of the JET methane

screening experiments and consequently had the most extensive DIVIMP and EDGE2D modeling and analysis.

The time evolution of the visible Bremsstrahlung Z_{eff} signals was similar to the JET experiment (fig. 1). The AUG carbon fuelling efficiency has about 20% uncertainty from the addition of all the sources of error in quadrature with the uncertainty in differencing the carbon content rise being the largest uncertainty. The JET fuelling efficiency has only about 15% uncertainty because the rise in Z_{eff} is larger making the differencing error less (Table I). The uncertainties in the measurements are similar between the two machines, although different systematic diagnostic errors may occur for similar diagnostics operated on different machines.

The results (Table I) indicate that AUG had a 27% higher fuelling efficiency than JET for methane injected at the horizontal mid-plane. Experimentally, the higher fuelling efficiency occurred because there was a higher carbon density increase in the AUG core for a similar injection rate of carbon. Although the Z_{eff} increase was smaller in AUG than JET, the higher AUG density meant that the carbon density increased more.

In section IV (Table II), EDGE2D predicts that AUG should have a 28% higher fuelling efficiency for 0.36 eV carbon injected at the horizontal mid-plane. For those simulations, a carbon diffusion coefficient of 0.5 m^2/s was used for both machines. The actual JET FE_{MP} quoted on Table II is the value as measured by the charge exchange system which was 30% lower than the value measured by the visible Bremsstrahlung diagnostic and quoted in Table I (see diagnostic discussion in [2]). Essentially, the carbon diffusion coefficient is a free parameter used to match the code results with the screening measurements, and in this paper, we have chosen to match the JET CX diagnostic for the screening. If we had chosen to match the VB diagnostic and the values in Table I, then a carbon diffusion coefficient of approximately 0.2 m^2/s would have been used (equation (9) in [2]). The use of different diagnostics for the carbon content in table I and II emphasizes the role of systematic uncertainties. Ref. [2] has a more thorough discussion of the JET uncertainties.

The conclusion from this section is that essentially the same EDGE2D model (identical transport coefficients, and Γ_D adjusted to match the experimental density) could account for the observed carbon fuelling efficiency simultaneously on both machines. This result supports the use of EDGE2D to identify size scaling effects.

III-EDGE2D MODELLING

EDGE2D is a predictive code [1] which solves the fluid equations in 2 dimensions for a given input power, deuterium gas fuelling rate, and set of transport coefficients. The code is coupled to a neutral Monte Carlo code, NIMBUS that tracks the neutral deuterium and carbon and their interactions with the vessel components. EDGE2D injects or sputters carbon as atomic carbon, and does not treat molecular processes. The code solves the edge plasma parameters self consistently. Each EDGE2D run uses the equilibrium from an actual discharge for JET or AUG, or a projected discharge for ITER. The equilibrium locates the grid cells along the magnetic surfaces of the discharge (Fig. 2). A small region of the plasma core and the divertor private flux region are followed. In the region from the edge of the grid to the vessel (the periphery), ions are presumed to decay with a 1 cm decay length. Those ions reaching the vessel walls are assumed to recycle locally as neutrals, which are tracked by NIMBUS.

The JET divertor is the Gas Box Divertor. The ASDEX divertor is the IIb Divertor. The ITER divertor is the V Divertor [11] which achieves the design power handling goal of 10 MW/m^2. Carbon is the only material used in the calculations. This might be acceptable for ITER if the tritium co-deposition issues were otherwise solved.

The JET grid (fig. 2) was wide enough to encompass the carbon ionization depth but also intersected some machine components, (RF antennae and the outer divertor baffle). Consequently, these components are ignored in the JET calculations. On the other hand, the ITER grid is narrower than the JET grid, since its equilibrium featured a second X-point just above the ITER vessel. The main consequence was that low energy carbon injected at the main chamber mid-plane could be ionized entirely at the grid edge, making for a poor calculation. Of the ITER cases, only one condition for mid-plane injected carbon was useful. In order to ionize the mid-plane injected carbon primarily within the SOL, 5 eV carbon injected into an ITER SOL heated by 15 MW (see Section IV) was required. Higher power or lower carbon energy resulted in most of the carbon being ionized at the grid edge. Injection into the divertor was unaffected by the grid size.

Our approach was to study the carbon behavior from four ensembles of EDGE2D runs:

1. Carbon was injected at the horizontal mid-plane of the main chamber vessel and no carbon sputtering was allowed. The arrows in figure 1 indicate the location of the carbon injection at the edge of the vessel (Section IV). This set of runs describes the screening of carbon injected at the outer mid-plane.

2. Carbon was injected near the outer strike point and no carbon sputtering was allowed (Section V). This set of runs describes the screening of carbon injected in the outer divertor.
3. Carbon occurred from the intrinsic physical sputtering and no carbon was injected, nor was chemical sputtering allowed (Section VI). This set of runs describes the carbon generation due to physical sputtering,
4. Carbon occurred from both physical and chemical sputtering but not from carbon injection (Section VI). Several cases were run with various chemically sputtered coefficients available in the literature [8-15]. The chemical sputtering was 10 to 20 times larger than the physical sputtering rates. The total sputtering rates scaled similarly, but not identical to the third ensemble of runs. This set of runs was used to describe the total intrinsic carbon influx.

These 4 data sets of EDGE2D runs identified the core contamination, the carbon flow pattern, and the carbon density pattern for each carbon source. For JET, individual runs scanned the potentially important input parameters and indicated which phenomena (besides device size) were important for the carbon behavior. The central condition around which these variations were based was the main L-Mode plasma of the JET carbon screening studies (Table II). It was a Gas Box diverted plasma at 2.5 MA heated by 2.5 MW neutral beams at 2 10^{19} /m^3 volume averaged density. The parameters varied included the transport coefficients, the SOL density, the energy of the injected carbon, the power into the SOL, and the chemical sputtering coefficient.

For each case, some difference in the SOL was achieved by each parameter variation. The deuterium particle diffusion coefficient (0.1, 0.5, or 1.5 m^2/s) controlled the SOL density width. Flat transport coefficients with zero pinch velocities were assumed. Higher deuterium injection caused larger SOL density but little change in the SOL density width (fig. 3), while smaller deuterium diffusion coefficient caused a narrower density width, and increased the core (and separatrix) density.

The ion and electron heat conductivities are assumed equal. The power flowing into the SOL (2, 2.5, 4, or 7 MW) influenced the SOL temperature. More power flowing into the SOL (fig. 3) caused higher SOL temperatures but little change in the SOL temperature width. The thermal heat diffusion coefficient (0.2, 0.75, or 1.5 m^2/sec) influenced the SOL temperature width. Lower heat conductivity caused a narrower temperature width as well as higher separatrix (and core) temperature.

The carbon diffusion coefficient (0.1, 0.5, or 1.5 m^2/s), the injection rate of carbon (if any was injected), the energy of the injected carbon (if any) (0.1, 0.36, 1.5, or 10 eV) directly influenced the carbon perpendicular transport, the carbon self-interactions and the location of the carbon ionization. Varying the injection rate of deuterium yielded mid-plane separatrix densities between 0.6 and 1.5 $10^{19}/m^3$. The chemical sputtering coefficient (if chemical sputtering was included) influenced the carbon generation rate, but did not influence the scaling between machines so long as the same coefficient was used for each machine.

The result was an ensemble of SOL conditions hopefully reflecting the range of JET plasmas. In part, the ensemble encompasses measurement uncertainties that exist in SOL measurements such as Langmuir probes, and partly, the ensemble allowed for plasma variations that might occur during specific experiments such as density and input power parameter scans. The difference between L-mode and H-mode is assumed only due to the higher power flowing into the SOL and the consequently higher SOL temperature. SOL transport has been assumed unchanged in the transition to H-Mode.

To understand the role of parallel distance to the divertor, JET equilibria from a q_{95} scan was used (q_{95} = 3, 4, or 5). Experimentally, the q_{95} scan was achieved by lowering the plasma current at constant magnetic field. In the actual experiment, the plasma current reduction was accompanied by increased core transport coefficients. The interpretation of the effect of parallel distance upon the carbon screening was difficult to isolate since the change in SOL transport coefficients was unknown, and not well measured on those plasmas [2]. However, with the code, the use of a different equilibrium with a different length to the divertor can be treated as a separate parameter, and identical transport coefficients, as well as the other input parameters were assumed, resulting in a clearer identification of the consequences of $L_{\parallel}$. This q_{95} scan in parallel length is one component of the size scaling study.

The other component is the modeling of AUG, and ITER, with major radius, minor cross-section, parallel length to the divertor, and the divertor size corresponding to each device. Most input parameters for the AUG and ITER cases were similar to the JET baseline case (table II) (D=.5 m^2/s, χ=.75 m^2/s, D_C=.5 m^2/s). These parameters were used to fit the JET experimental screening results. For AUG, the equilibrium was from the methane screening experiment (Section II). The deuterium fuelling was chosen to match the SOL density observed in that experiment, and the power was chosen to match the L-Mode power used. The transport coefficients were chosen equal to the JET baseline case, and reasonable agreement with the SOL

temperature and density profiles was obtained. Runs with different injected carbon energy were used to identify effects associated with the carbon ionization location.

The ITER plasmas had one of three powers: 15 MW, 50 MW, and 75 MW. 15 MW corresponds to ITER L-Mode, before tritium has been put into the device, while the 50 MW corresponds to a case near the H-Mode threshhold, and 75 MW corresponds to one possibility for the SOL power in the full DT burning experiment. In each case the transport coefficients were equal to the JET baseline case, and the gas puffing level was adjusted until the SOL density for the 75 MW case equaled the projected ITER density [6]. The 15 MW ITER separatrix temperature equals the JET and AUG separatrix values (fig. 4). At each ITER power level, the injected carbon energy (if any) was varied to scan the carbon ionization location.

In summary, EDGE2D was run to deduce the predicted carbon sputtering, screening, and flow and density patterns. The runs concentrated upon parameter scans centering on a JET baseline case. The JET baseline case was chosen for its agreement with the JET carbon screening experiments [2]. The importance of size will be deduced from similar runs using the baseline parameters from JET but with AUG and ITER equilibria.

IV MID-PLANE C INJECTION

While EDGE2D solves the appropriate fluid equations, the governing processes are not always evident, and so in this and the other sections, specific runs are used to isolate effects and thus interpret the code. The processes determining the main chamber, injected carbon evolution [2] are illustrated schematically in figure 5. The carbon is injected into the SOL from the wall region, either as physically sputtered neutrals, chemically sputtered hydrocarbons, as methane molecules in the case of carbon screening experiments, or as carbon neutrals in the case of EDGE2D calculations. For carbon injected into the main chamber, the carbon ionization rate peaks at a distance ρ (a few centimeters) from the separatrix. Carbon atoms ionized at that point contaminate the core on a time scale of $\tau_\perp = \rho^2/D_C$ by cross-field transport due to the impurity diffusion coefficient D_C. The core contamination is mitigated by parallel transport to the divertor. The parallel transit time is a fraction, ξ of the time, $\tau_\parallel$, that a typical carbon ion can move from one divertor entrance to the other: $\tau_\parallel = L_\parallel / V_C$, at the thermal carbon velocity V_C. Also important in the parallel transport is the thermal force which acts primarily near the separatrix at the divertor entrance and on higher charged carbon ions. The thermal force impedes the

escape of carbon into the divertor. In this section, these processes are quantified. The principal effects of machine size on the mid-plane screening are to change the distance from the separatrix that the carbon is ionized, the parallel distance to the divertor, and the magnitude of the thermal force.

The carbon ionization occurs inside the SOL for the mid-plane injected carbon (fig. 6). The peak of the ionization rate is a distance ρ from the separatrix. Higher energy carbon is ionized closer to the separatrix. The larger machine (i.e. ITER) has higher and wider SOL temperature due to the longer parallel length and higher power. Consequently, 5 eV carbon was ionized at a similar ρ in ITER, as .36 eV carbon in either JET or AUG, although with a wider distribution. EDGE2D runs with different carbon energy isolate the effect of ρ upon the carbon screening. In general, code runs like the JET case in figure 5 (having all the carbon ionized inside the SOL grid) probably yield more accurate screening results. However, grids wide enough to include all the ionization might also require modification of some machine components (Section III), and thus have other unrealistic aspects.

In general, the peak ionization is close enough to the separatrix that the characteristic perpendicular diffusion time, $\tau_\perp$ to the core was shorter than the parallel transit time for carbon to traverse the entire SOL from one divertor entrance to the other at the carbon thermal velocity (fig. 7). In terms of the data base of EDGE2D runs, the diffusive time scales are longer for lower carbon energy or carbon diffusion coefficient, while the parallel times were longer for longer $L_\parallel$, or lower SOL temperatures. When the carbon diffusion coefficient is assumed equal to the Bohm value (fig. 7), then the perpendicular and parallel time constants are correlated since both depend upon the SOL temperature.

The actual transit time from the mid-plane to the divertor will be shorter than the transit time between the divertor entrances, or $\xi < 1$. The carbon transit from the mid-plane to the outer divertor occurs in about º of $\tau_\parallel$ ($\xi =$ º). Also, the transit time where the flux expansion is small, and therefore the carbon is close to the core is shorter than $\tau_\parallel$, having $\xi = 0.2$. With these parallel transit times, much of the carbon injected at the mid-plane has sufficient time to diffuse to the core.

The JET carbon fuelling efficiency increased with longer parallel and shorter perpendicular times (fig. 8). Regression to the JET carbon fuelling efficiency indicated:

$$FE_{MP} = 0.02 \ln (\tau_\parallel / \tau_\perp) \qquad (1)$$

Our intention here and in later sections is to first deduce a JET scaling unrelated to machine dimensions. Then develop the size scaling by including the higher q_{95} JET, the AUG, and ITER cases. However, this method turns out to be more successful in the other sections than here. Regression with only the parallel and perpendicular time constants does yield a simple relation for the JET calculations (fig. 8). However, both the smaller and larger machines have higher fuelling efficiencies than JET at the same ratio of parallel to perpendicular time. Clearly, other phenomena are also important and complicate the scaling.

One important and complicated phenomenon is the thermal force. The thermal force acts strongest near the divertor entrance. The thermal force influences the higher charged particles preferentially (fig. 9), so that carbon can have a directed velocity of up to 40 km/s (fig. 10), while the deuterium is relatively unaffected. The force acts as a barrier, preventing carbon from reaching the divertor. The velocity peaks near the divertor entrance and near the separatrix, presumably due to the combined steep parallel temperature gradient and higher ionized carbon states. The width of the thermal force barrier relative to the divertor entrance may be associated with the SOL temperature width (fig. 4). However, we were unable to develop a simple relation or scaling characterizing the barrier.

Apparently, the carbon fuelling efficiency is more complicated than just the ratio of the parallel transit time to the perpendicular diffusion time (fig. 8). For carbon at 0.36 eV and $D_C = 0.5$ m^2/s, then the EDGE2D runs for AUG and JET are tabulated in Table II. For ITER, since the carbon would be ionizing beyond the edge of the grid, we estimated the mid-plane fuelling efficiency. The ITER mid-plane fuelling efficiency was estimated by the expected enhancement of $\tau_\perp$ if the carbon ionization were correctly located. From figure 3, 0.36 eV carbon ionization peak might occur about 8 to 10 cm from the separatrix if the temperature decay continued linearly from 4 cm (the edge of the ITER grid). The distance is so large because the far SOL region has a slow temperature decay and remains at high temperatures far from the separatrix. Consequently, the perpendicular time constant will be about 15 to 25 times longer than existed for the 5 eV, 15 MW ITER EDGE2D case that was actually calculated. Reducing the mid-plane injected carbon fuelling efficiency according to equation (1) means that 0.36 eV carbon will be screened about 5 to 6 times better than 5 eV carbon (fig. 11)

Defining the parallel transit time by the thermal velocity at the location of the carbon ionization peak, yields a size scaling for the fuelling

efficiency of 0.36 eV carbon injected at the mid-plane of the main chamber (fig. 11):

$$FE_{MP} = 3.1 / L_{\|} \qquad (2)$$

$L_{\|}$ is the parallel distance between the divertor entrances (in meters). The main chamber carbon screening becomes better linearly with larger machine size. However, that dependence may not be evident on single machine scans where the parallel length is increased (q_{95} scans) unless the SOL temperature is also varied accordingly. The primary physical effect is the higher SOL temperatures causing the carbon to be ionized further from the separatrix. The higher SOL temperatures are due both to higher power flowing into the SOL and the longer SOL temperature width (fig. 4).

EDGE2D also calculates the carbon exhaust location. The carbon can be lost to the inner divertor target, outer divertor target, or the wall. In EDGE2D, carbon reaching the grid edge is assumed lost to the wall. Thus carbon, quoted as lost to the wall, may experimentally be lost to the baffles just outside the divertor entrance (fig. 2). For carbon injected from the JET outer mid-plane, the fraction lost to the outer divertor increased with the carbon diffusion coefficient (fig. 12). The fraction of carbon lost to the inner divertor, or to the wall decreased with higher carbon diffusion coefficient. At constant diffusion coefficient, the fraction lost to the outer divertor leg becomes larger with longer parallel distance. We interpret figure 12 to indicate that the carbon can access the outer divertor leg more easily when it has moved to the outer SOL region. The higher diffusion coefficient, and the longer parallel distance help the outer mid-plane injected carbon to reach the outer SOL region. The thermal force is strongest at the outer divertor leg, and closest to the separatrix near the divertor entrance, so we think that these observations are an indication of the thermal force influencing the carbon migration.

V- OUTER STRIKE POINT CARBON INJECTION

A picture was developed of the divertor carbon screening using EDGE2D runs with carbon introduced only at the outer strike point. As in Section IV, the JET runs are used to identify the important physical processes. The carbon ionization is localized close to the outer strike point (fig. 13). Some carbon neutrals escape through the private region to the inner divertor leg, and some carbon neutrals escape to the main chamber SOL by passing from the outer strike point along the outer target face vertically into

the main chamber (fig. 13). The false color images of the carbon ionization rate pattern do not easily illustrate that the relative number of escaping carbon neutrals is small. This point is seen more clearly by observing the C^{++}, C^{+++}, and total carbon density. The carbon is concentrated along the field lines intersecting the strike point region (fig. 13). The C^{+++} density reaches further into the main chamber than the C^{++} density since ion motion is responsible for the movement of the carbon out of the divertor and into the main chamber SOL.

EDGE2D calculates the ion flux out of the divertor as well as the flux of escaping carbon neutrals which ionize in the main chamber SOL and core. Both fluxes decrease with increasing SOL density, and increase mildly with the injected carbon energy. The primary mechanism for carbon escape from the divertor is ion motion; being about 2 orders of magnitude larger than neutral escape from the JET divertor. The thermal force pulls the carbon ions out of the divertor and into the main chamber. The density dependence is due to the shorter carbon neutral mean free path from the outer strike point to the region of strong thermal force. The higher density makes it more difficult for carbon neutrals to reach the region of strong thermal force. The mild carbon energy dependence is due to a slightly longer ionization mean free path for the higher energy carbon.

The carbon fuelling efficiency (fig. 14) decreases at higher density and lower carbon energy. The fuelling efficiency for divertor carbon is relatively insensitive to the carbon diffusion coefficient in contrast to the fuelling efficiency for main chamber injected carbon (Section III). The core carbon fuelling efficiency has the same dependence on density and carbon energy as the carbon ion flux out of the divertor. The ITER values are significantly smaller than the JET values due to the approximately three times longer linear dimensions of the ITER divertor and the relatively unchanged thermal force imprint on the divertor (fig. 9). The AUG fuelling efficiency is lower than JET due to the higher density of the AUG case studied. The fuelling efficiency from the AUG divertor is lower than from the main chamber by a factor of 3 to 5. That ratio is similar to the JET experimental observation [2]. For the ITER divertor, the chance of a carbon escaping the divertor region as a neutral was negligible, and the core contamination was entirely due to ions escaping the divertor into the main chamber SOL and diffusing into the core.

A larger divertor or higher density operation caused better screening scaling approximately (fig. 14) as:

$$FE_{DIV} = .001 \{\ln (n_{sep} L_{DIV})\}^{-4} \qquad (3)$$

Where n_{sep} is measured in 10^{18} /m^3 and L_{DIV} (in m) is the distance from the X-point to the outer strike point and is used to characterize the linear dimension of the divertor. Equation (3) indicates that the relevant parameter is ratio of the carbon mean free path to the divertor size. However, the spatial variation of the EDGE2D calculated divertor parameters made calculation of the carbon mean free path difficult and equation (3) was not expressed in those terms. About 10% of the carbon reaching the main chamber SOL subsequently contaminated the core, independent of machine dimensions (fig. 15). ITER will screen divertor-released carbon a factor of 50 to 100 better than JET since the divertor linear dimensions are a factor-of-3 larger (fig. 14) resulting in a smaller fraction of carbon escaping the divertor.

Once the carbon from the strike point reaches the main chamber SOL, then its core fuelling efficiency is about twice as high as for the carbon injected at the mid-plane (Section IV). The thermal force acts nearer the separatrix than the place where the mid-plane injected carbon was ionized. The carbon density at the divertor entrance (fig. 16) is peaked much closer to the separatrix than for the mid-plane injected carbon. Consequently, divertor injected carbon has higher core fuelling efficiency once it reaches the main chamber SOL.

To summarize this section: the screening of carbon injected at the outer strike point is improved by higher density or larger divertor size (equation (3)). Modeled ITER results indicate carbon fuelling efficiencies 50 to 100 times lower than JET values. The basic physical process is the removal of carbon from the divertor by the thermal force. The basic phenomenon controlling the fuelling efficiency is the efficiency for carbon ionization in the region where the thermal force influences the carbon motion.

VI ñ CARBON SPUTTERING

In this section, the size scaling of the EDGE2D calculated sputtering rates is developed. Implicit to this section, is the assumption that the wall components and conditioning are similar to the JET walls. For example, the common JET algorithm [7] for the impurity source is a carbon wall and divertor with a chemical sputtering yield of 0.5 of the Toronto value [8]. The factor of Ω was proposed in Ref. [7] to account for the JET carbon light signals and may represent either a calibration factor in the JET instrumentation or the sputtering coefficients. This assumption, with the

empirical screening, predicts JET carbon core contamination similar to the experimental values [2]. The EDGE2D sputtering rates predicted for AUG and ITER, are as if they were constructed of the same carbon material conditioned to the same state as JET. In other words, these EDGE2D calculations predict the carbon source dependence upon machine size, at constant wall conditions. Two EDGE2D calculations were run: one with physical sputtering only, and another with both physical and chemical sputtering. Of particular importance is the dependence of the sputtering upon the magnitude of the incident deuterium flux [9]. The common JET algorithm is to use a sputtering coefficient [8] which is not reduced at increased particle fluxes, as many other sputtering coefficients are [10-15]. Consequently, the projections to ITER, which has relatively larger deuterium fluxes hitting its targets, may be overestimates. However, the issue is complicated since EDGE2D indicates that the dominate contamination does not arise from the location of the largest deuterium bombardment (see following paragraphs). This paper has isolated upon the role of machine size in the absence of flux dependence.

For all three machines, the carbon sputtering is primarily located in the divertor. Both physical and chemical sputtering are strong near the inner and outer strike points in JET (fig. 18). For both AUG and ITER, the sputtering is largest near the strike point but also extends up the target and into the divertor entrance.

The carbon density patterns inside the divertor are different for the 3 machines (Fig. 17). For JET, the carbon density is peaked along the field lines intersecting the strike point. The AUG pattern is largest along the length of the target. The particular AUG case used here has high density and consequently is relatively more dominated by chemical sputtering than the JET or ITER cases (Table II). For ITER, the intrinsically sputtered carbon density peaks a distance displaced up the target. The ITER pattern being shifted away from the strike point is calculated to be an effect of the temperatures along the target increasing away from the strike point. The effect was stronger and the displacement higher at higher power. This effect is probably the consequence of the divertor design which is intended to trap neutrals near the strike point, essentially plugging the divertor with plasma [6]. Clearly, these different patterns of carbon divertor density are a difficulty for scaling the screening and core contamination due to divertor sources between different machines. One issue is that the ITER displacement may be dependent upon machine operating conditions. In this paper, different operation conditions were simulated by the parameter variations in

the JET cases. Since the displacement was not seen in JET cases, the treatment here may not account for the appropriate variations.

Compared to JET, ITER has more of the sputtered carbon ionized in the divertor (85 to 95%), than JET (80 to 85%) (fig. 19). While JET has 5 to 8% of the sputtered carbon ionized in the main chamber SOL, ITER has only about 1%. ITER generally contains the sputtered carbon better inside the divertor chamber than JET.

The scaling of the total sputtering rate was slightly different than the scaling of the physical sputtering (fig. 20) with power flowing into the SOL being important for both. Chemical sputtering was about ten times larger than physical sputtering except for AUG, where the chemical sputtering was approximately 20 times larger than the physical sputtering. The chemical sputtering dominated the scaling for the total sputtering rate (fig. 20). Regression indicated that the physical sputtering rate, Γ_{phys} in carbons/sec, was increased with power into the SOL measured in MW, and with the length of the strike point, parameterized here as the length of the X-point, R_X in m:

$$\Gamma_{phys} = 10\ P^{2/3}\ R_X^{3/2} \qquad (4)$$

While the total sputtering rate, Γ_{tot} in carbons/sec, regressed to equation (5) where L_{DIV} is measured in m, n_{sep} is measured in 10^{18} /m^3, and the power into the SOL, P, is measured in MW:

$$\Gamma_{tot} = 150\ L_{DIV}\ (n_{sep}\ P)^{1/2} \qquad (5)$$

One interesting feature of equationís (4) and (5) is the role of the size parameters. Size acts in two ways, one is that increasing size increases the wetted surface area available for carbon release, and the other is that power densities are reduced acting to lower target temperatures. Apparently, the regressions indicate that EDGE2D calculates that the former effect is stronger. Larger divertor size, L_{DIV}, increases the chemical sputtering rate, plausibly because there is more carbon surface to react chemically. A longer strike point, R_X, increases the physical sputtering, again plausibly by increasing the carbon exposure to energetic particle bombardment. Also, increased density increases the chemical sputtering rate, again plausibly by increasing the bombardment of carbon surfaces and allowing more chemical reactions to occur. However, the improved screening at higher density and

larger divertor size (Section IV) means that increasing machine size (and especially divertor size) does lead to less core contamination.

The carbon ionization rate in the main chamber SOL is an indication of the carbon source originating from the wall. However, that rate may also include carbon originating in the divertor but near the divertor entrance. The main chamber SOL ionization rate scaled as:

$$\Gamma_{SOL} = 30\ \Gamma_D\ a\ b\ /\ n_{SEP} \qquad (6)$$

where a and b are the core plasma width and height in m, so ab is proportional to the cross-sectional area. Γ_D is the injection rate of deuterium required to achieve the separatrix density and is measured in deuterons/sec. Equation (6) indicates that lower deuterium fuelling efficiency leads to more carbon ionization in the SOL. Equation (6) is a consequence of EDGE2D assuming that the wall source is released by charge exchange. The carbon ionization rate in the main chamber SOL rises with increasing deuterium flux to the wall, as evidenced by the Γ_D dependence.

Another significant observation from the EDGE2D runs was that the pattern of impurity sources was different on the three machines. The peak ITER carbon influx was tens of cm from the strike point in contrast to JET where it was at the strike point. The carbon fuelling efficiency increased by a factor of 7 to 12 when the carbon was injected 30 to 50 cm vertically up the target from the outer strike point in a separate EDGE2D run where that was the only carbon source (fig. 21). That distance caused the carbon density to have a similar pattern as the intrinsic 75 MW ITER carbon density (*i.e.* fig. 18: 75 MW ITER and fig. 21 are similar). Apparently, the ITER divertor fuelling efficiency is complicated by significant carbon being released closer to the divertor entrance than the strike point. Probably in anticipation of this result, the present ITER design mitigates this carbon source by switching the target material to tungsten in this vicinity.

Further, the ITER equilibrium used here (fig. 2) would have a high sputtered source near the machine top that was not calculated by EDGE2D. The ITER SOL is much hotter than for JET, and in particular the grid edge had much higher temperatures. Consequently, the ITER wall near the machine top would experience ion bombardment that was not calculated by these EDGE2D models.

VII ñ CARBON CONTENT

The carbon content arises from the sum of all the significant impurity sources. Following the approach used with JET [2], only two sources of carbon - the main chamber walls and the divertor, are considered:

$$N_C = (FE_{MP}\,\Gamma_{wall} + FE_{DIV}\,\Gamma_{DIV})\,\tau_p^* \qquad (7)$$

The total carbon content of the core, NC, is obtained using FE_{MP} from equation (2), FE_{DIV} from equation (3), Γ_{wall} from equation (6), Γ_{DIV} from equation (5), and $\tau_p^* = a\,b\,/\,4\,D_C$ as defined by the core carbon diffusion coefficient.

One consequence of the development here is that we can isolate the relative contribution of the divertor and the wall as the source of core contamination. Essentially, the wall contributes about a constant carbon number independent of machine size (fig. 21) while the divertor contribution decreases with larger divertor size and higher operating SOL densities. On JET, the divertor contribution can equal the wall contribution while for ITER the wall contribution is significantly larger. However, as discussed in Section V, the ITER divertor may actually contribute significantly to the main chamber SOL carbon ionization due to the importance of carbon emission displaced away from the strike point.

The carbon content (fig. 22) can be expressed in terms of the physical processes:

$$N_C\,/\,(\Gamma_{tot}\,\tau_p^*) = 0.1\,(\Gamma_{SOL}/\Gamma_{tot})\,/\,(L_{\parallel}\,n_{SEP}^{1/2}) \qquad (8)$$

The carbon content increases trivially if the sputtering rate or core confinement increases. At fixed sputtering rate and core confinement, the carbon content increases if the fraction of carbon ionizing in the main chamber SOL increases, or the length to the divertor decreases, or the density decreases.

While equation (8) expresses the carbon content in terms of the relevant physical processes, the same results can also be expressed in terms of the EDGE2D input parameters (fig. 23).

$$Z_{eff}\,\tilde{n}\,1 = 0.25\,(P/n_{sep})^{3/2}\,/\,\{L_{DIV}^{\,2}\,D_C^{\,1/2}\} \qquad (9)$$

The carbon content, Z_{eff} -1 increases with power flowing into the SOL measured in MW, and decreases at higher SOL density measured in $10^{18}/m^3$, larger divertor chamber size measured in m, and higher carbon diffusion coefficient measured in m^2/s. The use of divertor size in equation (9) is

rather arbitrary, and might be better expressed as a general machine linear dimension.

CONCLUSIONS

EDGE2D calculations indicate the importance of machine size upon the carbon contamination. We studied an ensemble of JET runs to isolate the important parameters besides machine size, and coupled that to specific AUG and ITER calculations assigning residual effects to machine size. This approach was undertaken since EDGE2D reasonably described JET screening and intrinsic impurity experiments.

The screening of carbon injected into the main chamber has several inter-connected size related effects. Probably, the most significant difference between the ITER and JET SOL is that ITER will have a higher separatrix temperature due to the higher power flow into the SOL. Also the SOL temperature will be wider due to the longer parallel length to the divertor. Both effects act to move the carbon ionization further from the separatrix, and reduce fuelling efficiency. ITER will better screen carbon originating from the main chamber than JET, about in proportion to the parallel length to the divertor.

The screening of carbon injected into the divertor is easier to understand. The carbon moves out of the divertor and into the main chamber SOL as ions accelerated by the thermal force. Size scaling acts principally on the ability of the carbon neutrals to reach the region where the thermal force dominates. Since this is a mean free path process, then high density operation, as for the AUG discharge modeled here, can be as effective as divertor size at keeping carbon from reaching the main chamber SOL and thus the core. ITER might be 100 times better at screening divertor carbon sources than JET (see Table II for the projected screening, sputtering, and core contamination).

The screening of physically or chemically sputtered carbon should be similar to the cases studied of carbon injection at the mid-plane or at the outer strike point. The actual core contamination expected for ITER depends upon the material components chosen for the ITER construction, and the flux dependence of the sputtering yields (taken as zero in this paper). If ITER were composed of the same carbon material as JET and if it behaved in the same way, then the scaling of the ITER sputtering rate would increase with power flowing into the SOL and decrease with SOL density.

ACKNOWLEDGEMENTS

The authors thank G. Sips, A. Loarte, and J. Rapp for help with generating the ITER and AUG grids. This work was supported by EFDA. JDS was supported by the U.S. DOE. The help of the ASDEX Upgrade experimental team is gratefully acknowledged.

REFERENCES:
[1] R.Simonini, *et al*, Contrib. Plasma Phys. **34**, 368 [1994]
[2] J.D.Strachan, *et al*, Nuclear Fusion **43**, 922 [2003]
[3] K.Lackner, Comments Plasma Phys. Controlled Fusion **15**, 359 [1994]
[4] P.C.Stangeby, and J.D.Elder, J. Nucl. Mater. **196-198**, 258 [1992]
[5] O. Gruber, *et al*, Nuclear Fusion **41**, 1369 [2001]
[6] A.S.Kukushkin, *et al*, Nuclear Fusion **42**, 187 [2002]
[7] H.Y. Guo, *et al*, Nuclear Fusion **40**, 379 [2000]
[8] A.A.Haasz, B.V.Mech, and J.W.Davis, J. Nucl. Mater. **231**, 170 [1996]
[9] M. Lehnen, private communication
[10] C.Garcia-Rosales and J. Roth, 21st EPS Conf. on Controlled Fusion and Plasma Phys. Montpellier [1994] p. II-770
[11] A.Pospieszczyk, *et al*, J. Nucl. Mater. **241-243**, 833 [1997]
[12] V. Philipps, *et al*, J. Nucl. Mater. **313-316**, 354 [2003]
[13] A.A.Haasz and J.W.Davis, J. Nucl. Mater. **224**, 141[1995]
[14] J.Roth, Garcia-Rosales, Nuclear Fusion **36**, 1647 [1996]
[15] J.Roth, JNM **266-269**, 51 [1999]
[16] A.Geier, *et al*, PPCF **44**, 2091 [2002]

Figures Captions:

Figure 1. Time evolution of Zeff measured by visible bremstrahlung for AUG and JET. The time scale is normalized to the average energy confinement time.

Figure 2. The EDGE2D grids used for AUG, JET, and ITER. The arrows point to the location of the carbon injection used to analyze the screening properties of each machine. The solid arrows indicate where experimental results exist (Section II and ref. [2]).

Figure 3. EDGE2D predicted JET SOL temperature and density profiles at the outer mid-plane for cases where thermal heat conductivity, power into the SOL, deuterium particle diffusivity, and the injection rate of deuterium were varied separately.

Figure 4. EDGE2D predicted SOL temperature for AUG, 2 power levels of ITER, and the baseline JET case in Table II.

Figure 5. Schematic diagram indicating the principal processes influencing the carbon injected into the main chamber [2]. The SOL consists of two regions: the region close to the divertor where the time to diffuse to the core is less than the time to parallel transport to the divertor and the outer region where the parallel time is shorter. At the divertor entrance, and close to the separatrix, the thermal force acts to impede carbon transport to the divertor.

Figure 6. The ionization rate for carbon injected at the horizontal mid-plane plotted against the distance from the separatrix.

Figure 7. The characteristic perpendicular diffusion time scale from the peak of the carbon ionization to the separatrix plotted against the characteristic parallel carbon transit time of the entire main chamber SOL. τ_{CLOSE} is the parallel transit time for carbon to transverse the region of small flux expansion where the field lines are close to the separatrix.

Figure 8. The carbon fuelling efficiency plotted against the regression expression of equation (1) as a function of the ratio of the parallel to perpendicular characteristic times.

Figure 9. Vector plots of the JET deuterium flow, the JET carbon flow, the AUG carbon flow, and the ITER carbon flow for L-Mode plasmas from the 3 machines.

Figure 10. The C^{+++} flow velocity calculated at the divertor entrance.

Figure 11. The carbon fuelling efficiency plotted as a function of parallel length for $D_C = 0.5\ m^2/s$, and $E_C = 0.36$ eV. The line indicates equation (2). The two ITER cases are based upon the projected location of the carbon ionization for 15 and 75 MW (Section IV).

Figure 12. The exhaust location for carbon injected at the JET outer mid-plane plotted as a function of the carbon diffusion coefficient. Anomalous SOL flows which occur in JET would direct more carbon towards the inner divertor leg.

Figure 13. False color images (white is highest, and dark is lowest) of carbon ionization rate, C^{++} density, C^{+++} density, and total carbon density for the JET standard case are plotted. The only carbon in the EDGE2D calculation was .36 eV carbon injected at the outer strike point.

Figure 14. The carbon fuelling efficiency for carbon injected at the outer strike point plotted against the natural logarithm of the product of divertor size with separatrix density. The line indicates equation (3).

Figure 15. The carbon fuelling efficiency plotted against the fraction of ions reaching the main chamber SOL for carbon injected at the outer strike point.

Figure 16. The JET C^{+++} density at the divertor entrance, for EDGE2D runs where the carbon was injected at the outer strike point at .36 and 10 eV, or injected at the outer mid-plane at .36 or 10 eV. The points are the grid locations and the lines connect the points.

Figure 17. False color images of the sputtered carbon ionization rates.

Figure 18. False color images of the total carbon density for sputtered carbon.

Figure 19. The fraction of carbon ionized in the main chamber SOL plotted against the fraction ionized in the divertor. For JET, 5 to 10% of the sputtered carbon in ionized in the main chamber SOL, while 80 to 85% is ionized inside the divertor. For ITER, about 1% of the sputtered carbon is ionized inside the main chamber SOL while 85 to 95% is ionized inside the divertor.

Figure 20. The total sputtering rate (chemical + physical) plotted against the regression fit of equation (5). The scaling of the physically sputtered carbon is similar to that of the total rate due to the similar power and size dependence in equation (4), but is lower by about an order of magnitude.

Figure 21. False Color image of the total carbon density with carbon injected at the outer target but displaced 40 cm above the strike point.

Figure 22. The core contamination caused by carbon ionized in the main chamber SOL plotted against the core contamination caused by carbon ionized inside the divertor and moved by ion transport into the main chamber.

Figure 23. The carbon content of the core plasma plotted against the regression of equation (8). The EDGE2D runs had both physical sputtering and chemical sputtering [8].

Figure 24. The value of Z_{eff}-1.0 from the calculated data also plotted in figure 23. The carbon content is plotted against the regression of equation (9).

Table I. The experimental results from AUG and JET. The methane was injected at the horizontal mid-plane.

quantity	**units**	**AUG exp**	**JET exp**
shot		16300	49705
Plasma		H^+	D^+
gas		CH_4	CD_4
Γ_C	10^{21} /s	1.5	1.7
ΔZ_{eff}		.3	.8
$<n_e>$	10^{19} /m^3	6.2	2.4
Volume	m^3	14.4	80
τ_E	s	0.075	0.5
n_{sep}	$10^{19}m^{-3}$	2.0	.94
FE_{MP}	%	7.9	6.2

Table II. EDGE2D results from runs with $D = D_C = 0.5\ m^2/s$, and $\chi_i = \chi_e = 0.75\ m^2/s$. The JET EDGE2D run had agreement with the experimental charge exchange measured screening from 49705 which was the extensively modeled discharge in [1]. The D_{Bohm} value was calculated at the mid-plane separatrix. $L_{\|}$ is the parallel length between the divertor entrances. R_X is the major radius of the X-point and is meant to characterize the length of the strike point by averaging the inner and outer strike point major radii. L_{DIV} is the distance from the X-Point to the outer strike point and is meant to characterize the size of the divertor. The ratio of mid-plane to diverted injected screening is similar to that calculated by DIVIMP for tungsten on AUG [16].

quantity	units	AUG	JET	ITER	ITER
P_{SOL}	MW	2	2.5	15	75
R_X	m	1.4	2.7	5.1	5.1
P_{SOL}/ R_X	MW/m	1.3	.9	3	15
$L_{\|}$	m	65	70	170	170
L_{DIV}	m	0.25	0.3	1.25	1.25
T_{sep}	eV	102	85	92	178
n_{sep}	$10^{18}m^{-3}$	17.3	9.4	7.5	26.3
D_{Bohm}	m^2/s	1.55	1.28	1.37	2.58
Γ_{phys}	$10^{19}/s$	23.4	63.2	333	1283
Γ_{tot}	$10^{19}/s$	361	348	1902	$1.3\ 10^4$
Z_{eff}	Physical sputtering	1.06	1.21	1.48	1.13
Z_{eff}	total sputtering	1.33	1.58	1.56	2.06
FE_{DIV}	%	0.0018	0.68	0.0027	0.012
FE_{MP}	%	5.5	4.3	1.8	1.5

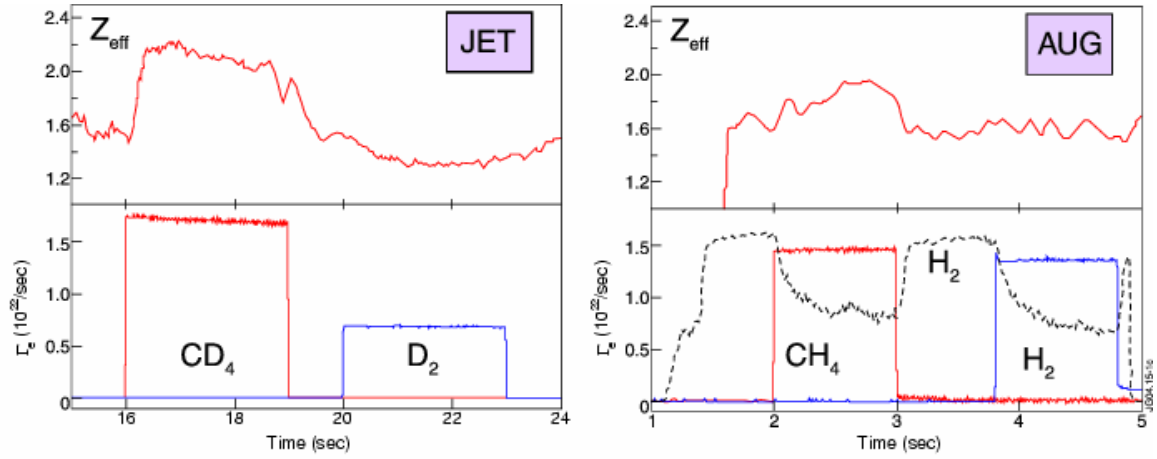
JET
Z_{eff}
2.4
2.0
1.6
1.2
1.5
1.0
0.5
0
Γ_e (10^{22}/sec)
CD_4
D_2
16
18
20
22
24
Time (sec)
AUG
Z_{eff}
H_2
CH_4
H_2
1
2
3
4
5
Time (sec)

Figure 1

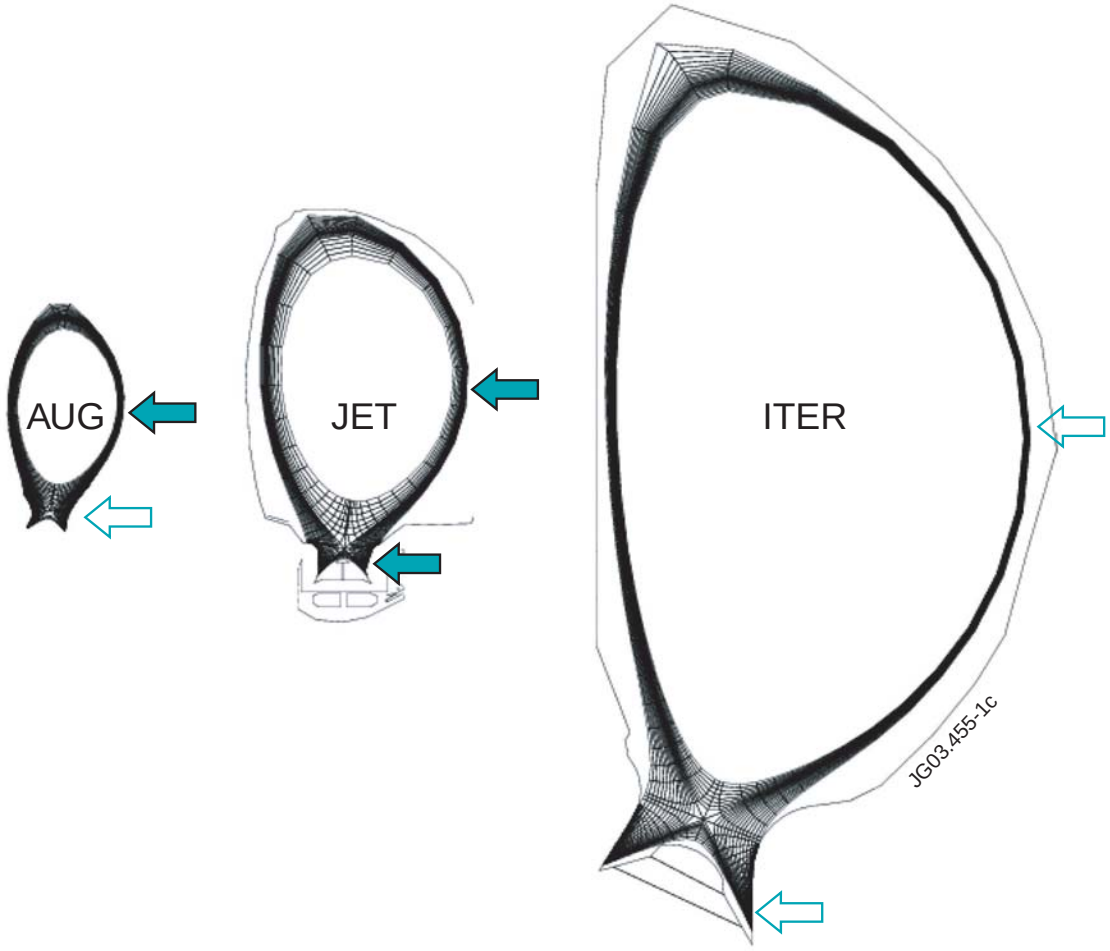

Figure 2.

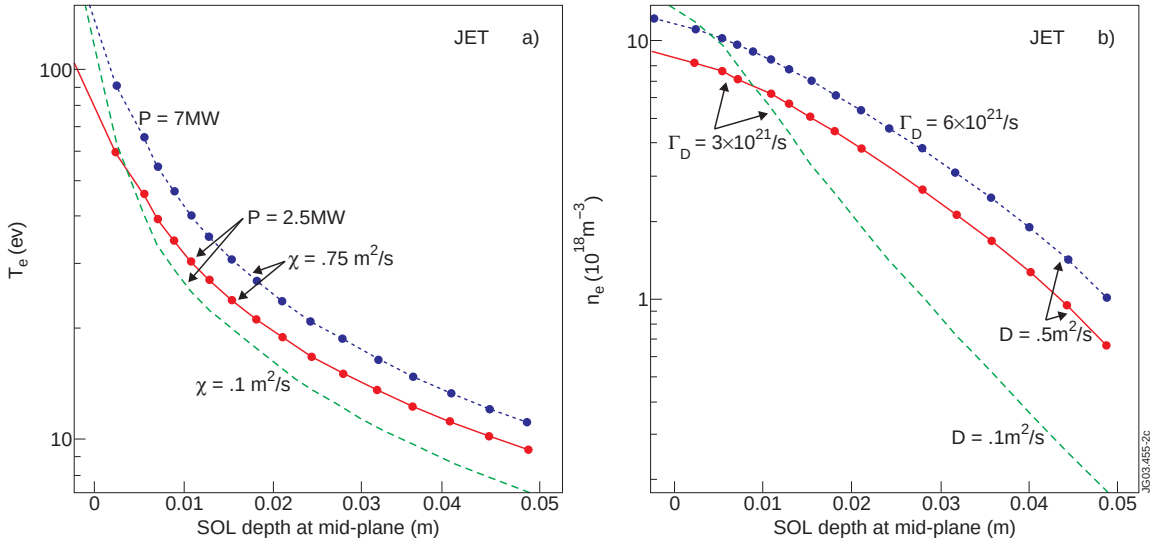
JET a)
100
10
P = 7MW
P = 2.5MW
χ = .75 m²/s
χ = .1 m²/s
T_e (ev)
0
0.01
0.02
0.03
0.04
0.05
SOL depth at mid-plane (m)
JET b)
10
1
Γ_D = 6×10²¹/s
Γ_D = 3×10²¹/s
D = .5m²/s
D = .1m²/s
n_e (10¹⁸m⁻³)
SOL depth at mid-plane (m)
JG03.455-2c

Figure 3

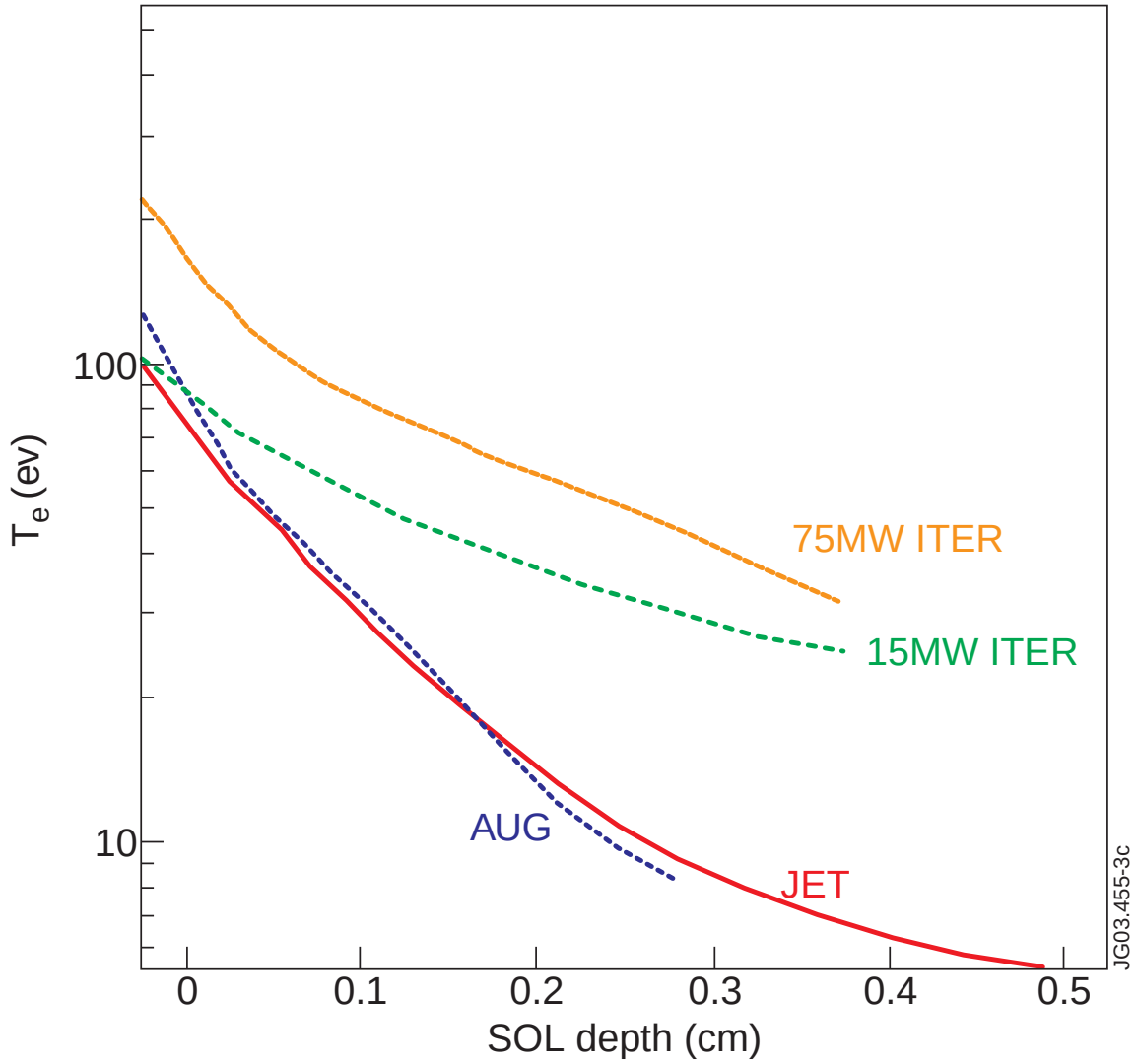
100
10
T_e (ev)
75MW ITER
15MW ITER
AUG
JET
0
0.1
0.2
0.3
0.4
0.5
SOL depth (cm)
JG03.455-3c

Figure 4

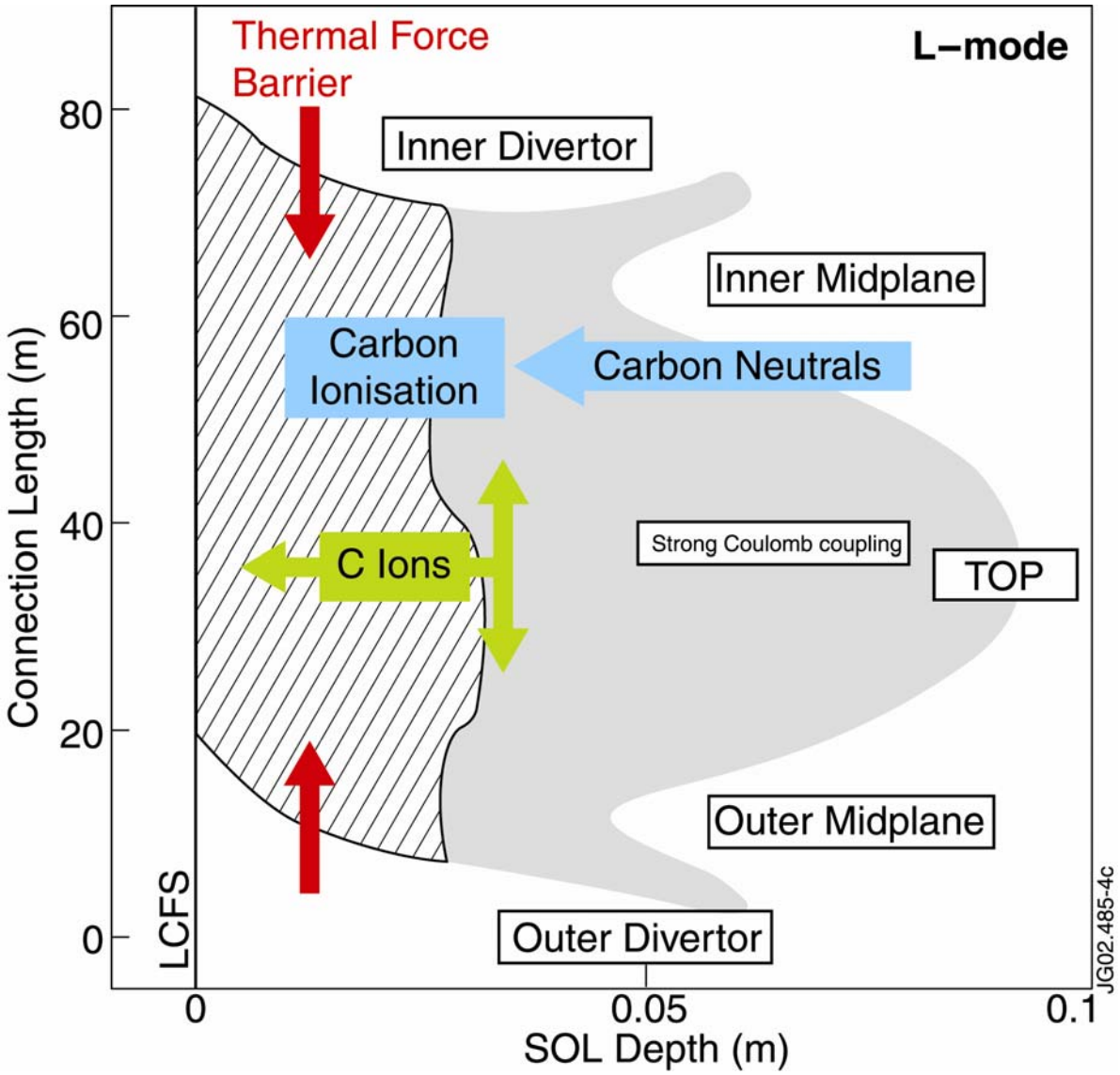
Thermal Force
Barrier
L–mode
Inner Divertor
Inner Midplane
Carbon
Ionisation
Carbon Neutrals
C Ions
Strong Coulomb coupling
TOP
Outer Midplane
Outer Divertor
LCFS
Connection Length (m)
80
60
40
20
0
0
0.05
0.1
SOL Depth (m)
JG02.485-4c

Fig. 5

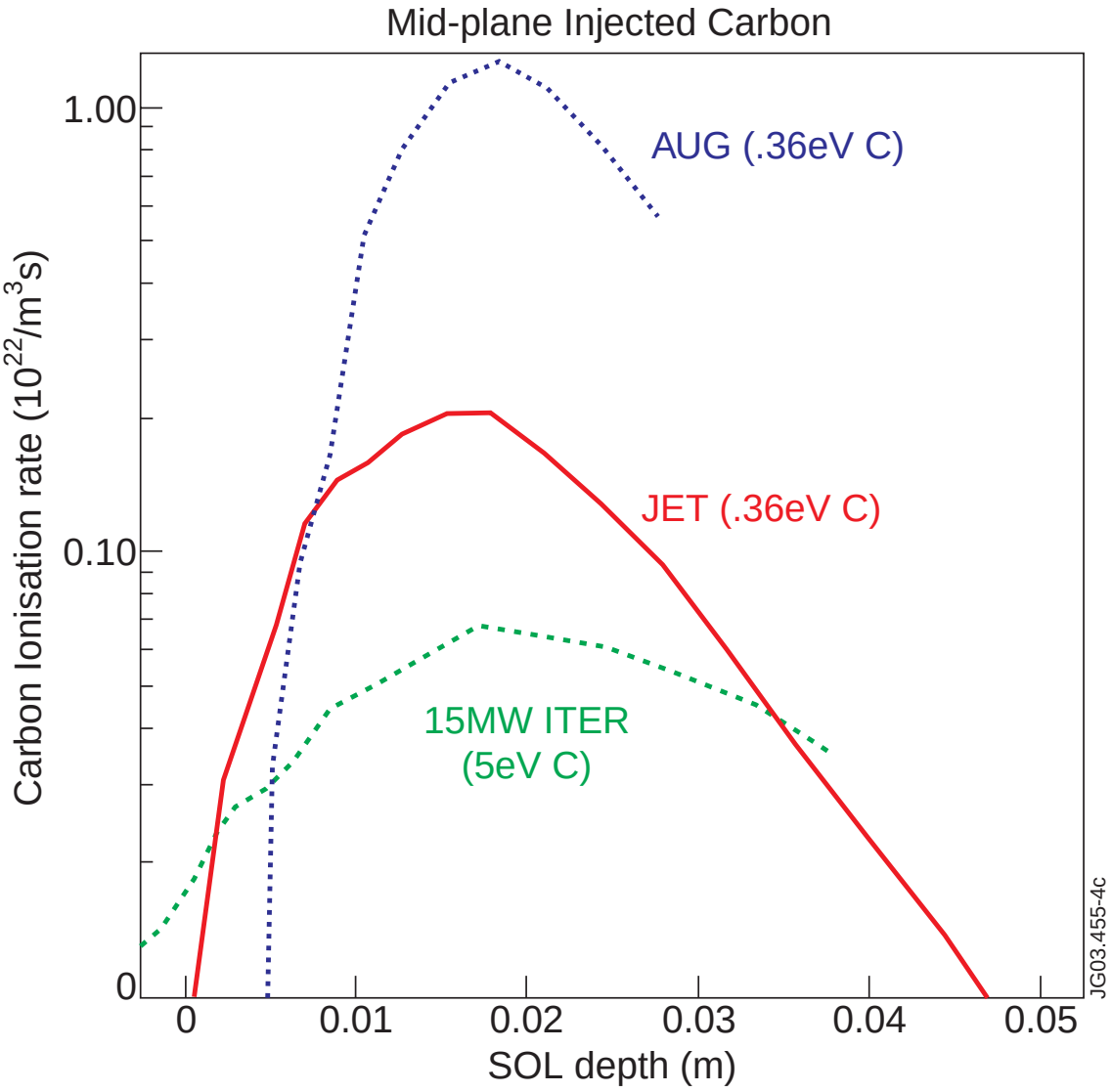
Mid-plane Injected Carbon
1.00
0.10
0
Carbon Ionisation rate (10^{22}/m^{3}s)
AUG (.36eV C)
JET (.36eV C)
15MW ITER
(5eV C)
0
0.01
0.02
0.03
0.04
0.05
SOL depth (m)
JG03.455-4c

Figure 6.

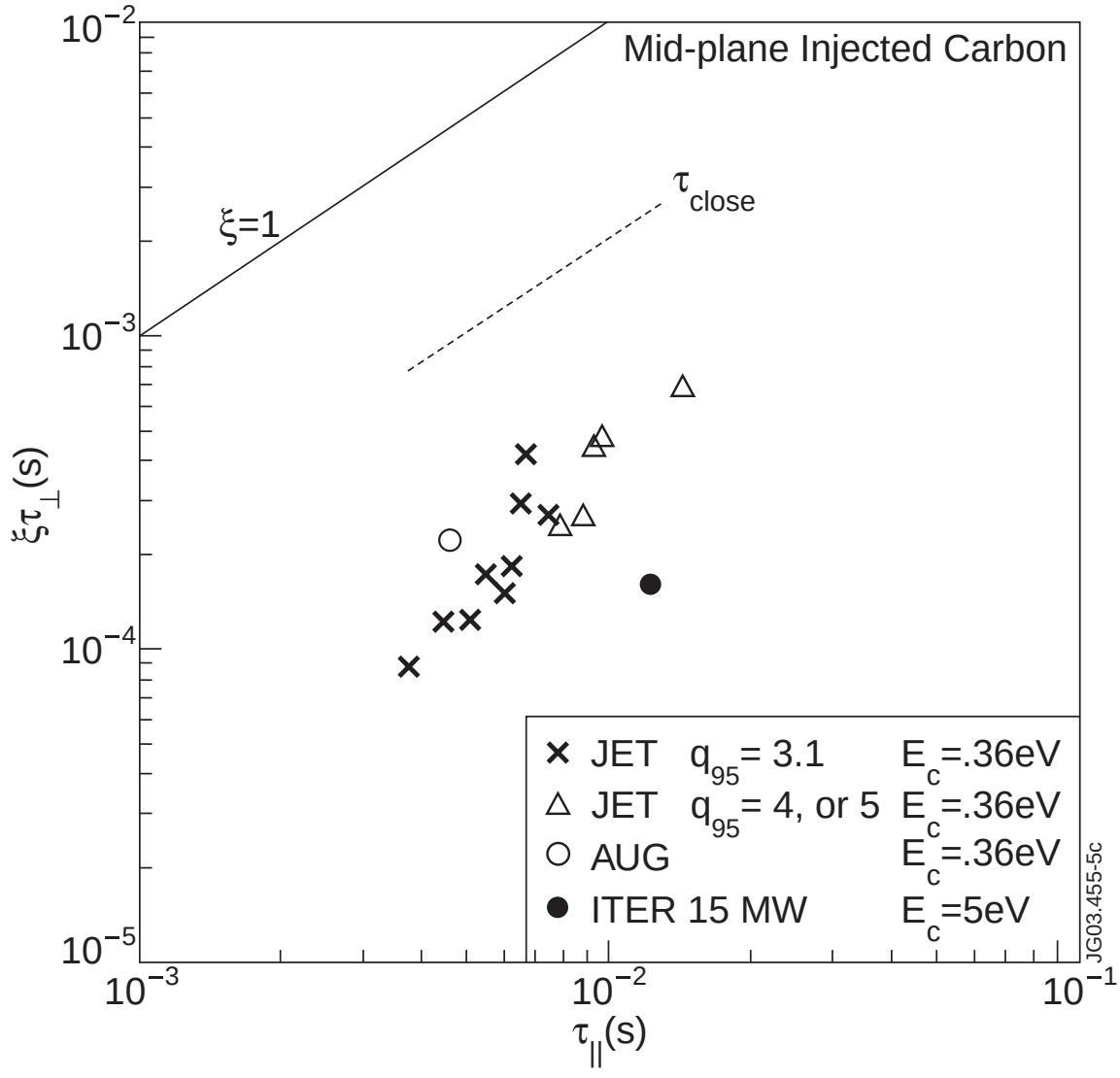
Mid-plane Injected Carbon
ξ=1
τclose
ξτ⊥(s)
τ||(s)
JET q95= 3.1 Ec=.36eV
JET q95= 4, or 5 Ec=.36eV
AUG Ec=.36eV
ITER 15 MW Ec=5eV
JG03.455-5c

Figure 7.

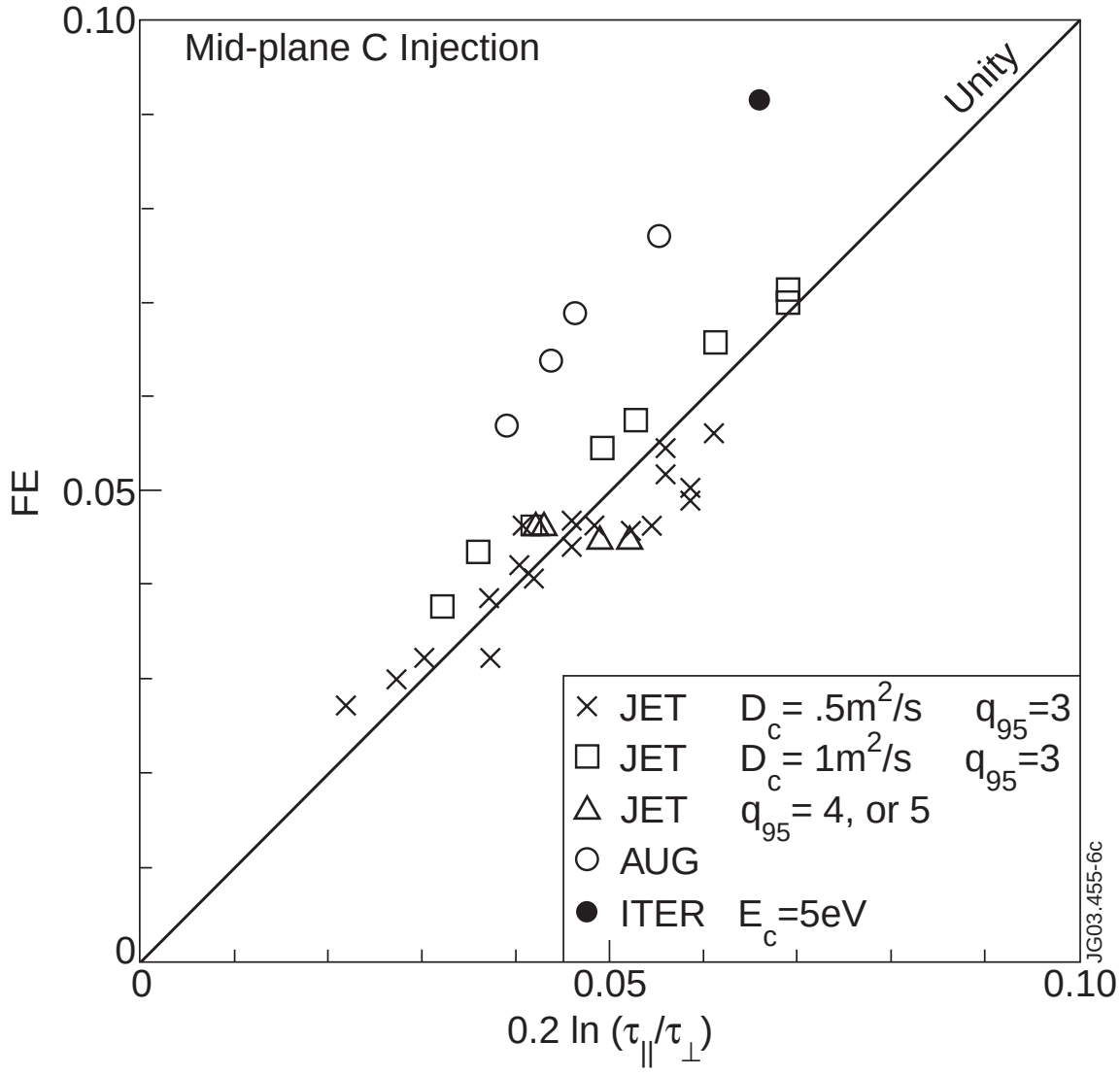
Mid-plane C Injection
Unity
FE
0.10
0.05
0
0
0.05
0.10
0.2 ln (τ||/τ⊥)
JET Dc= .5m2/s q95=3
JET Dc= 1m2/s q95=3
JET q95= 4, or 5
AUG
ITER Ec=5eV
JG03.455-6c

Figure 8.

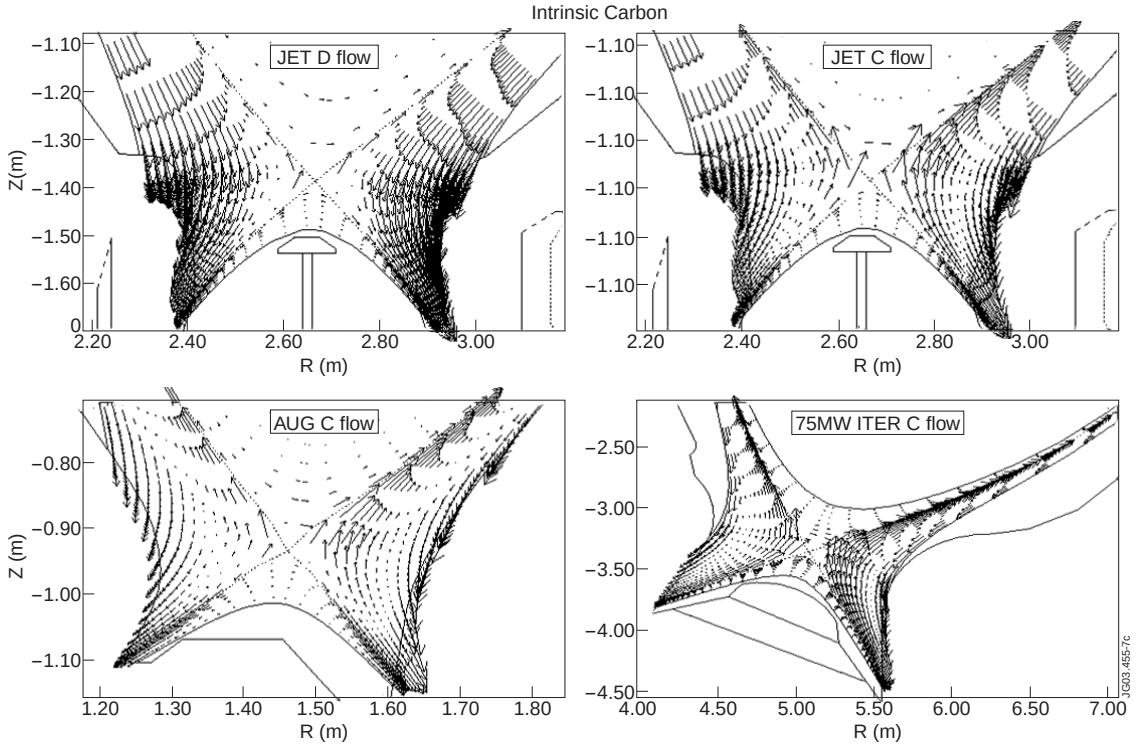
Intrinsic Carbon
JET D flow
JET C flow
AUG C flow
75MW ITER C flow
Z(m)
Z (m)
R (m)
JG03.455-7c

Figure 9.

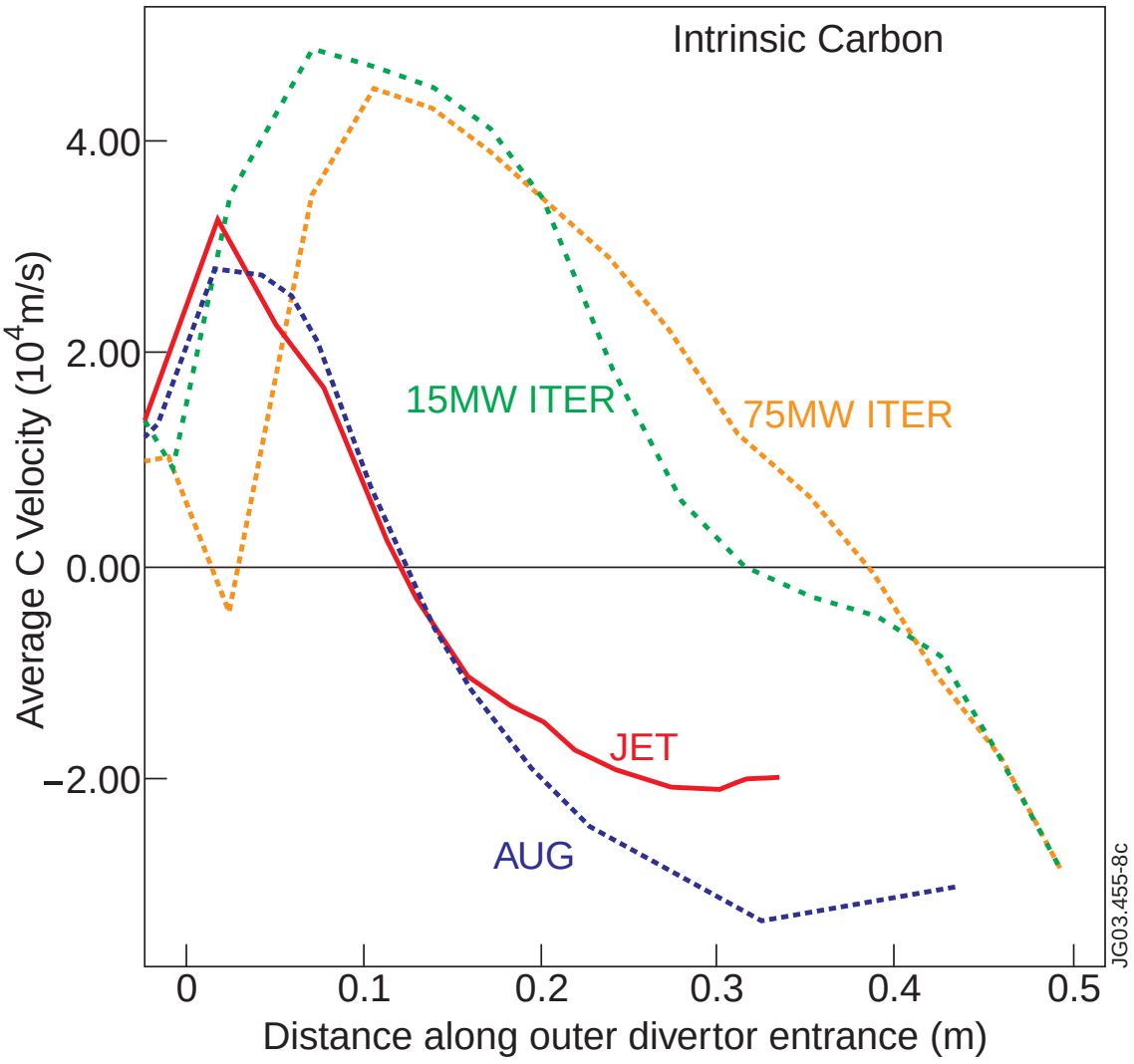
Intrinsic Carbon
4.00
2.00
0.00
−2.00
Average C Velocity (10^4m/s)
15MW ITER
75MW ITER
JET
AUG
0
0.1
0.2
0.3
0.4
0.5
Distance along outer divertor entrance (m)
JG03.455-8c

Figure 10.

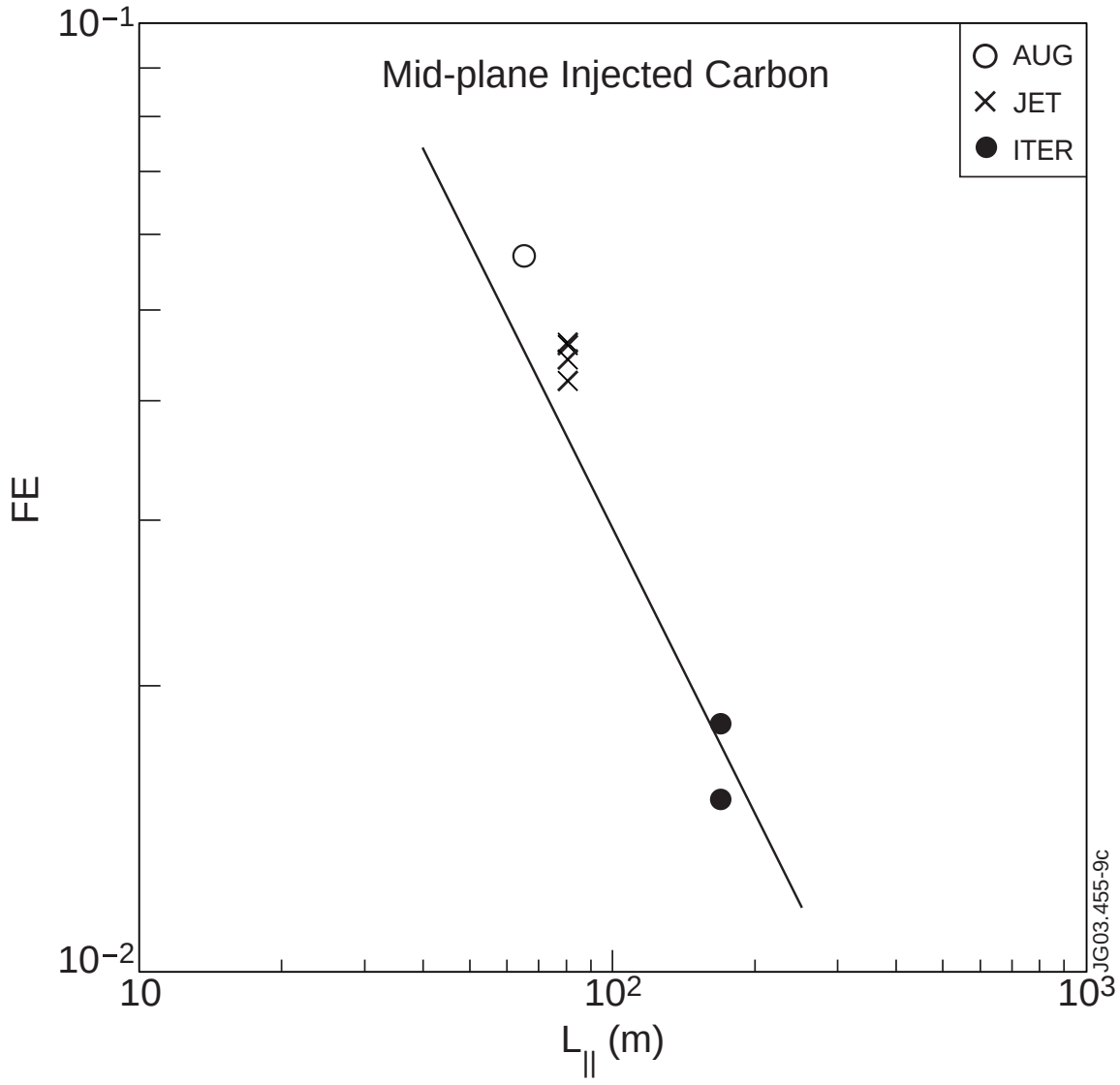
Mid-plane Injected Carbon
AUG
JET
ITER
FE
10^{-1}
10^{-2}
10
10^2
10^3
$L_{||}$ (m)
JG03.455-9c

Figure 11.

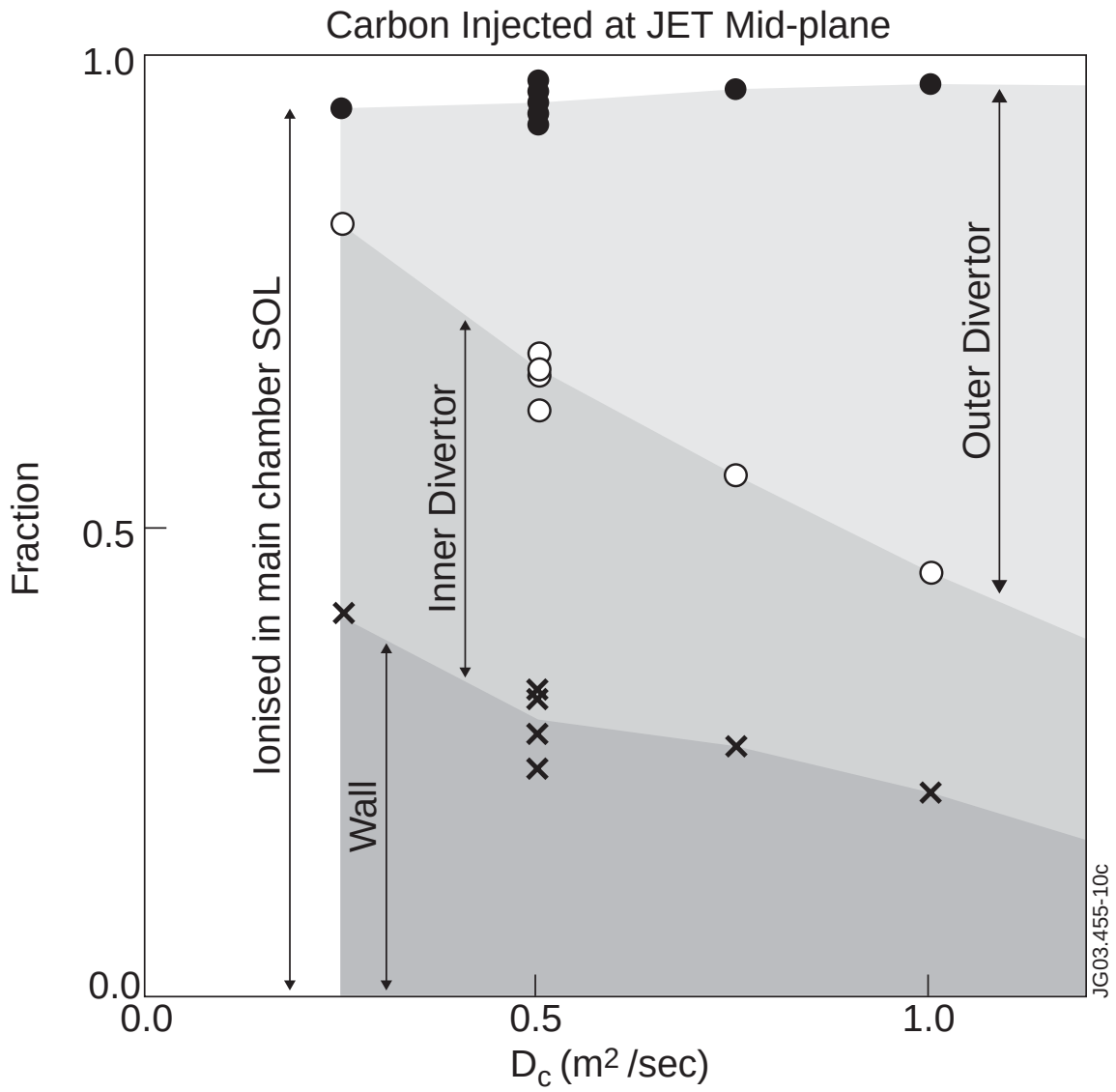
Carbon Injected at JET Mid-plane
1.0
0.5
0.0
Fraction
Ionised in main chamber SOL
Inner Divertor
Outer Divertor
Wall
0.0
0.5
1.0
D_c (m^2 /sec)
JG03.455-10c

Figure 12.

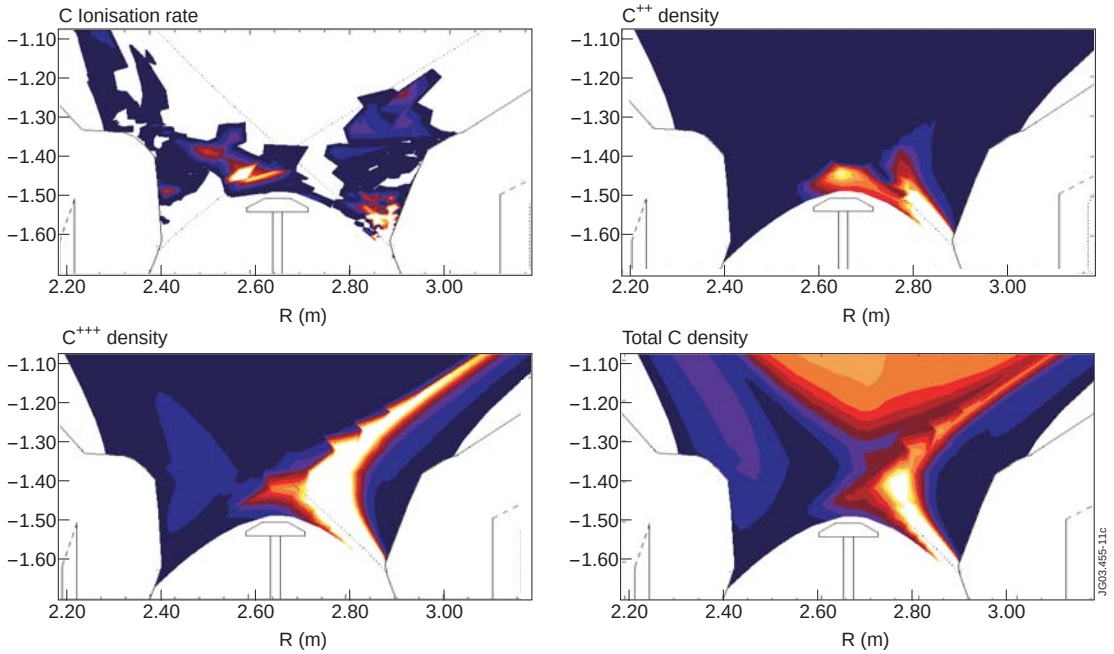
C Ionisation rate
C++ density
C+++ density
Total C density
−1.10
−1.20
−1.30
−1.40
−1.50
−1.60
2.20
2.40
2.60
2.80
3.00
R (m)
JG03.455-11c

Figure 13.

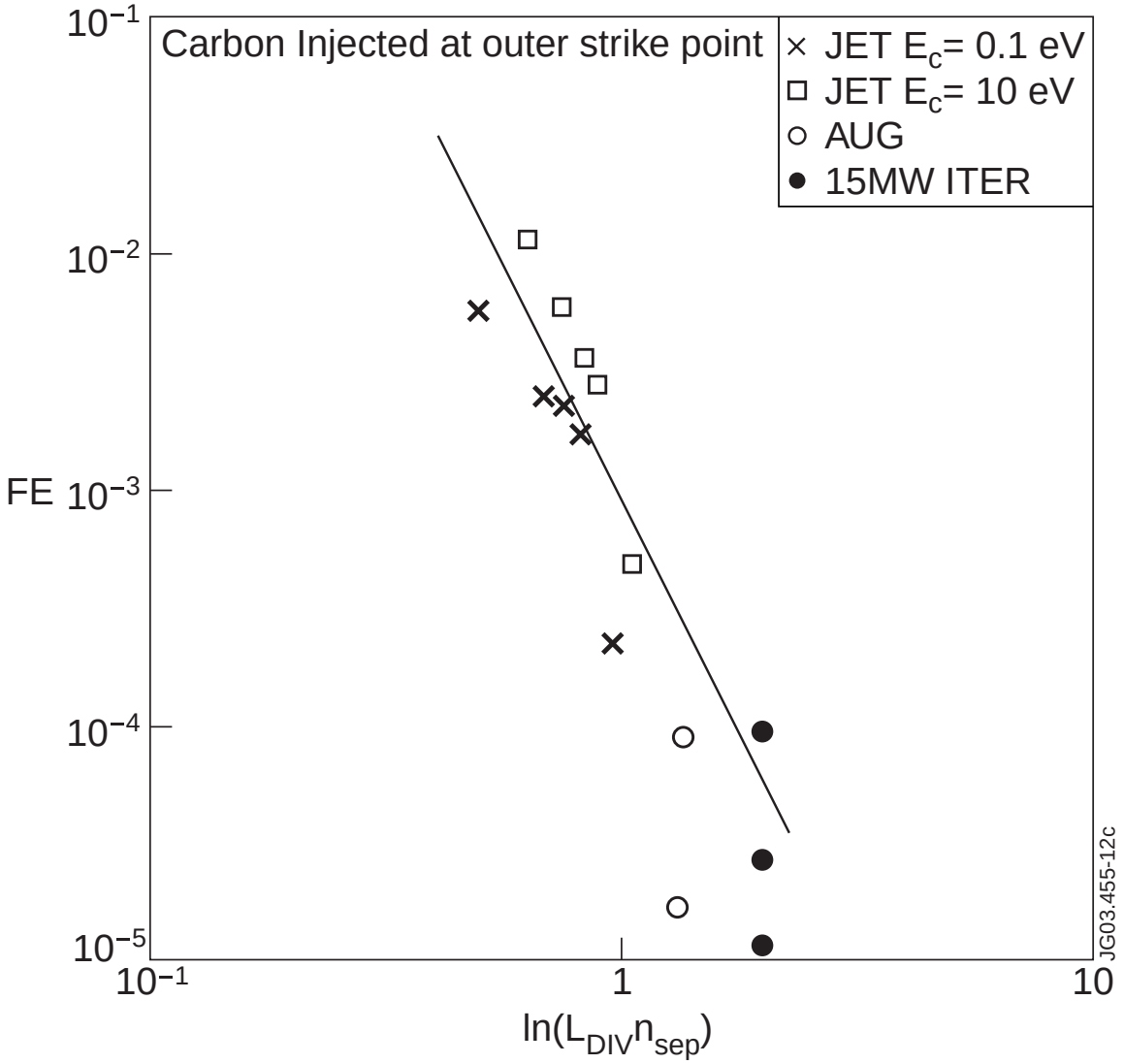
Carbon Injected at outer strike point
× JET E_c= 0.1 eV
□ JET E_c= 10 eV
○ AUG
● 15MW ITER
FE
10^{-1}
10^{-2}
10^{-3}
10^{-4}
10^{-5}
10^{-1}
1
10
$\ln(L_{DIV}n_{sep})$
JG03.455-12c

Figure 14.

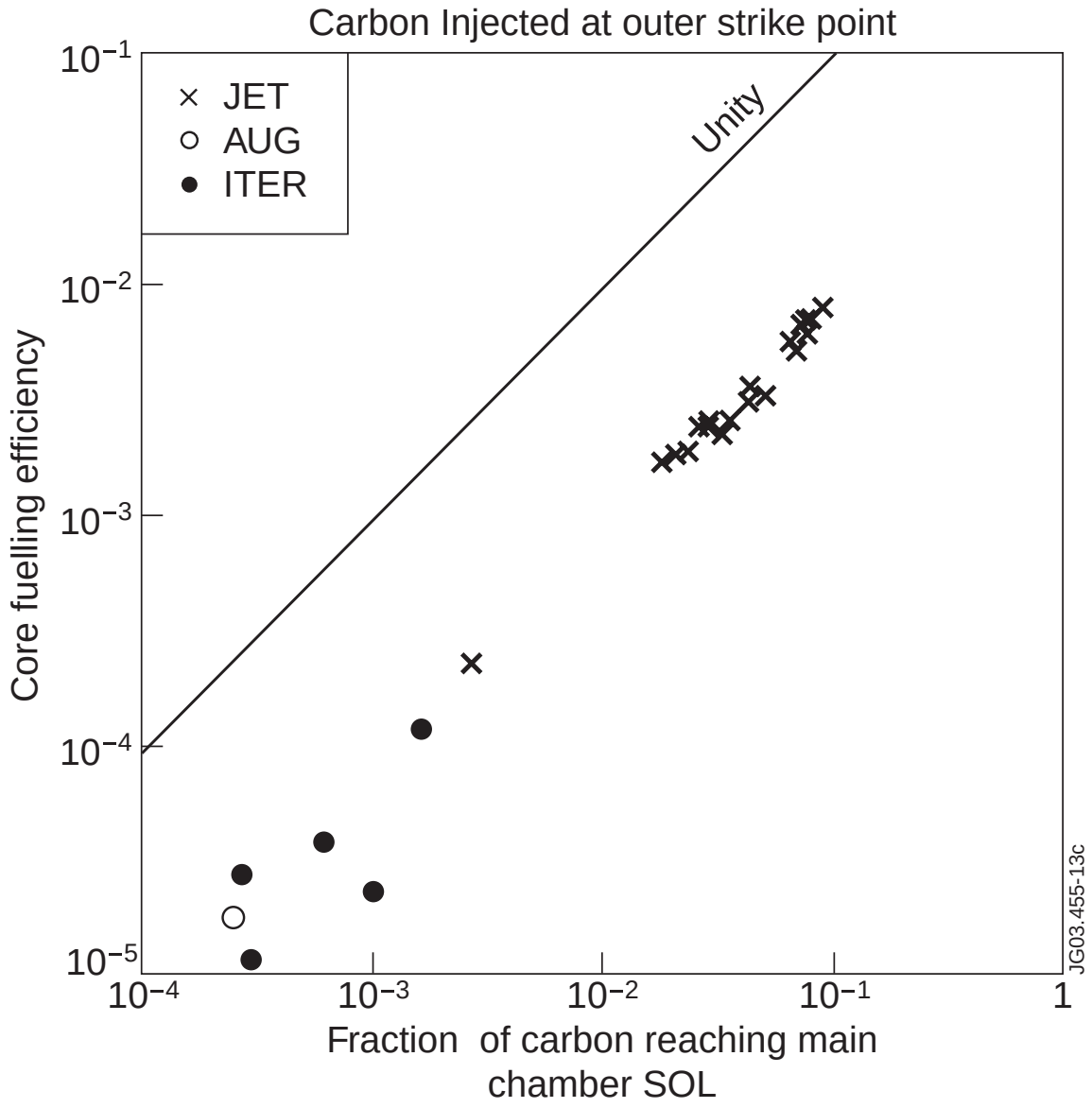
Carbon Injected at outer strike point
JET
AUG
ITER
Unity
Core fuelling efficiency
Fraction of carbon reaching main chamber SOL
JG03.455-13c

Figure 15.

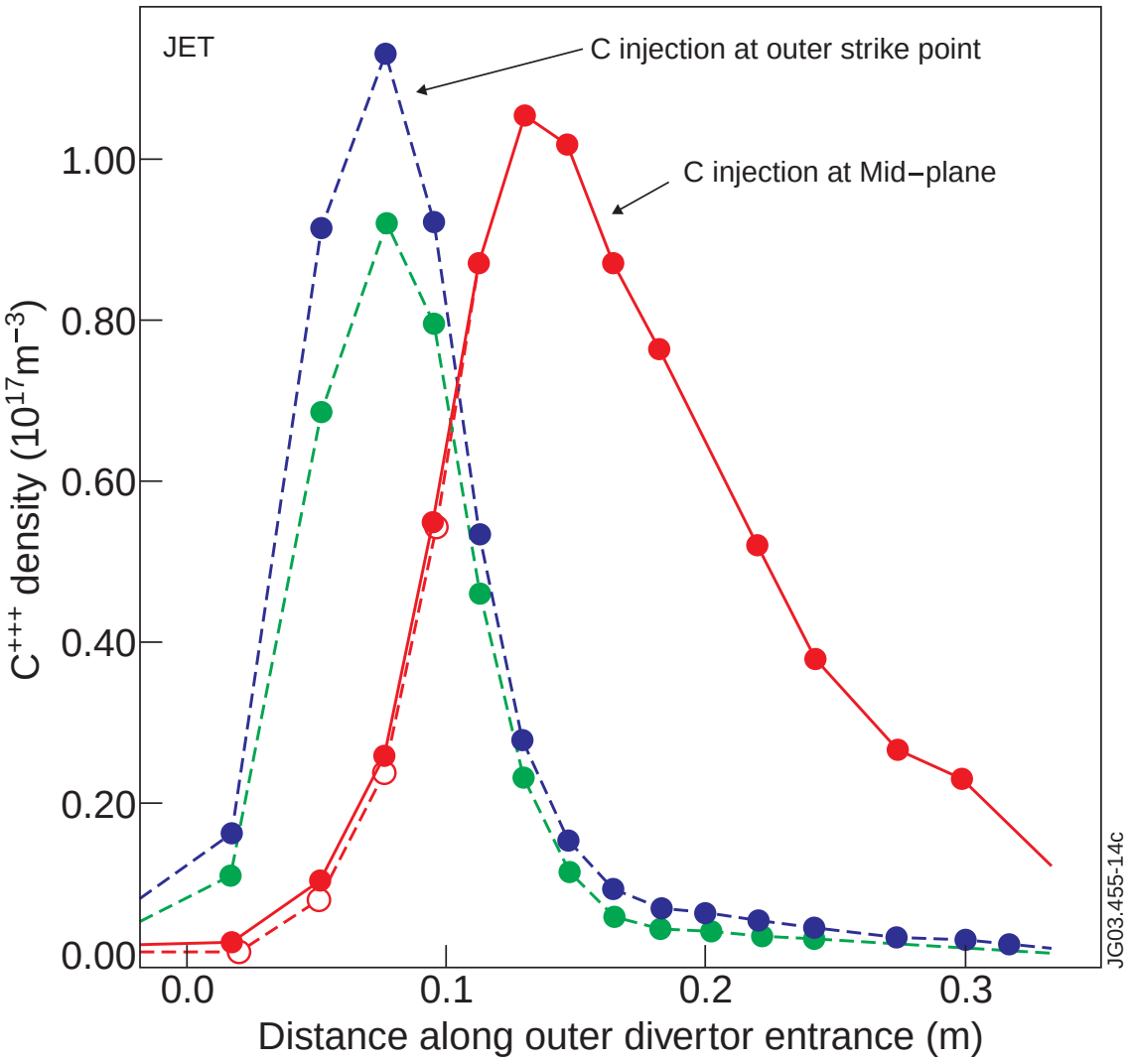
JET
C injection at outer strike point
C injection at Mid−plane
1.00
0.80
0.60
0.40
0.20
0.00
C+++ density (10^17 m^−3)
0.0
0.1
0.2
0.3
Distance along outer divertor entrance (m)
JG03.455-14c

Figure 16.

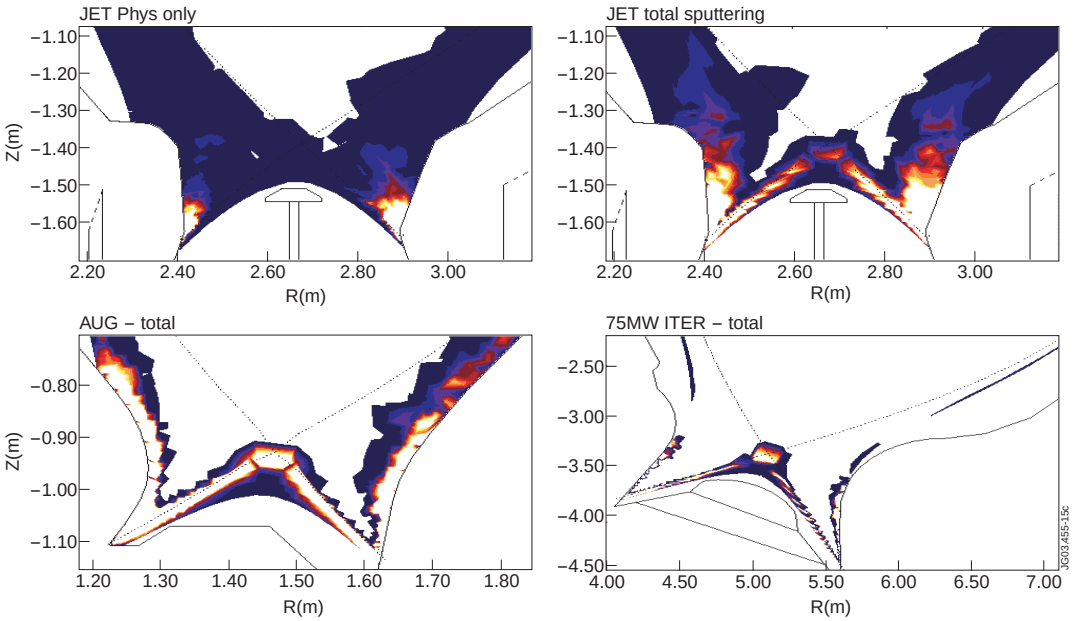
JET Phys only
JET total sputtering
AUG – total
75MW ITER – total
Z(m)
R(m)
JG03.455-15c

Figure 17.

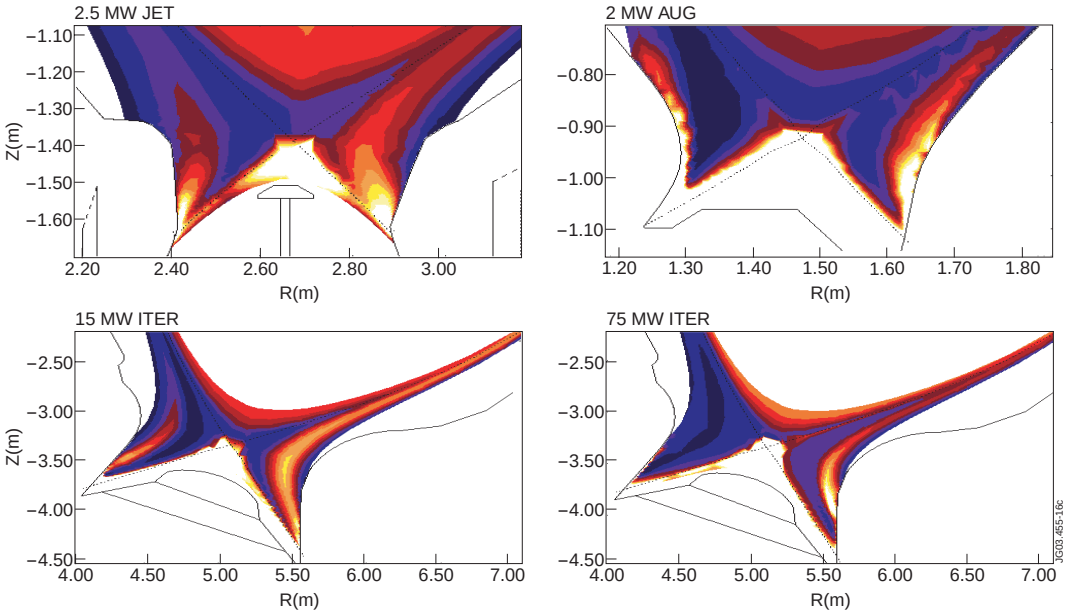
2.5 MW JET
2 MW AUG
15 MW ITER
75 MW ITER
Z(m)
R(m)
−1.10
−1.20
−1.30
−1.40
−1.50
−1.60
2.20
2.40
2.60
2.80
3.00
−0.80
−0.90
−1.00
−1.10
1.20
1.30
1.40
1.50
1.60
1.70
1.80
−2.50
−3.00
−3.50
−4.00
−4.50
4.00
4.50
5.00
5.50
6.00
6.50
7.00
JG03.455-16c

Figure 18.

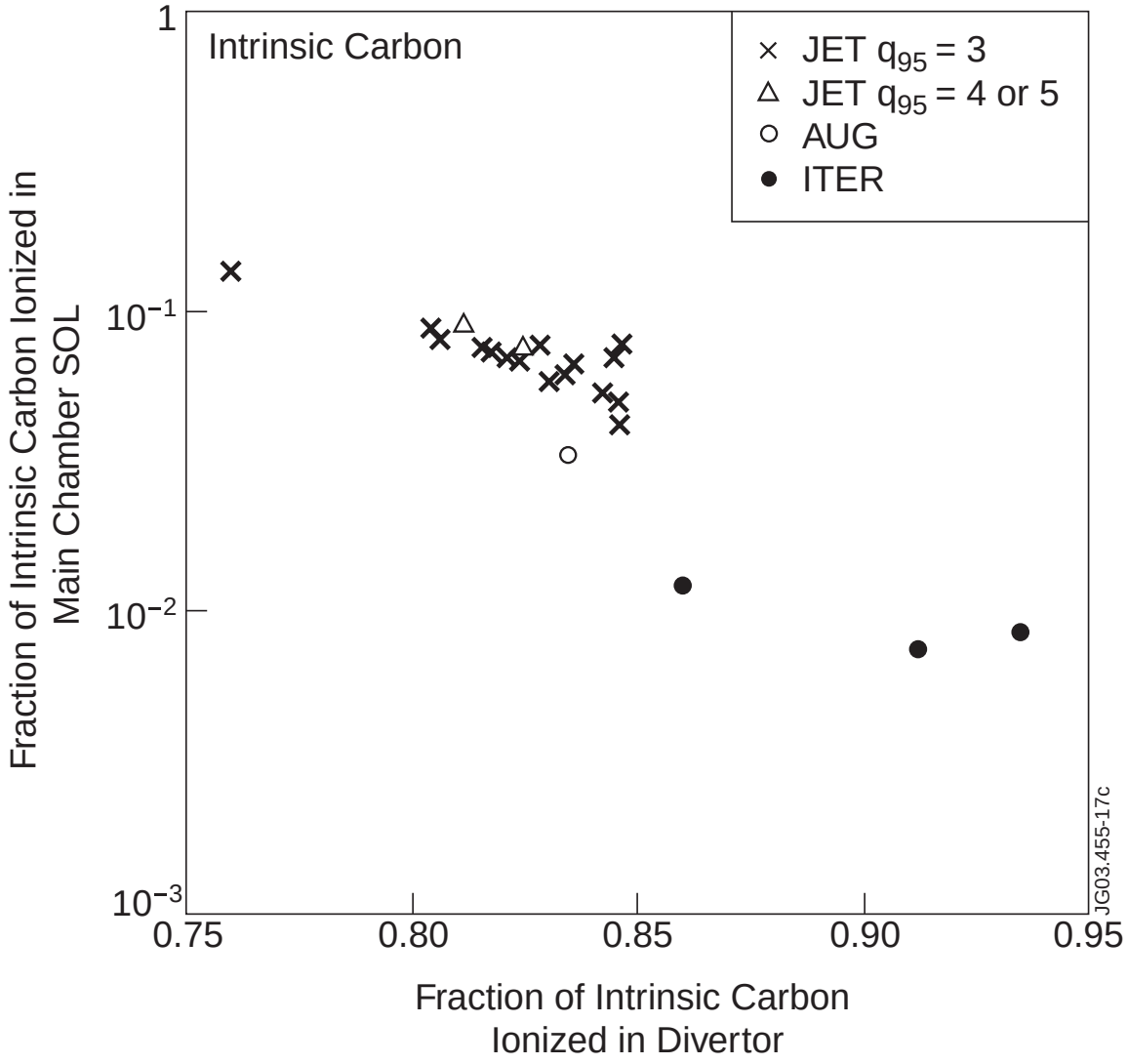
Intrinsic Carbon
× JET q_{95} = 3
△ JET q_{95} = 4 or 5
○ AUG
● ITER
Fraction of Intrinsic Carbon Ionized in Main Chamber SOL
1
10^{-1}
10^{-2}
10^{-3}
0.75
0.80
0.85
0.90
0.95
Fraction of Intrinsic Carbon Ionized in Divertor
JG03.455-17c

Figure 19.

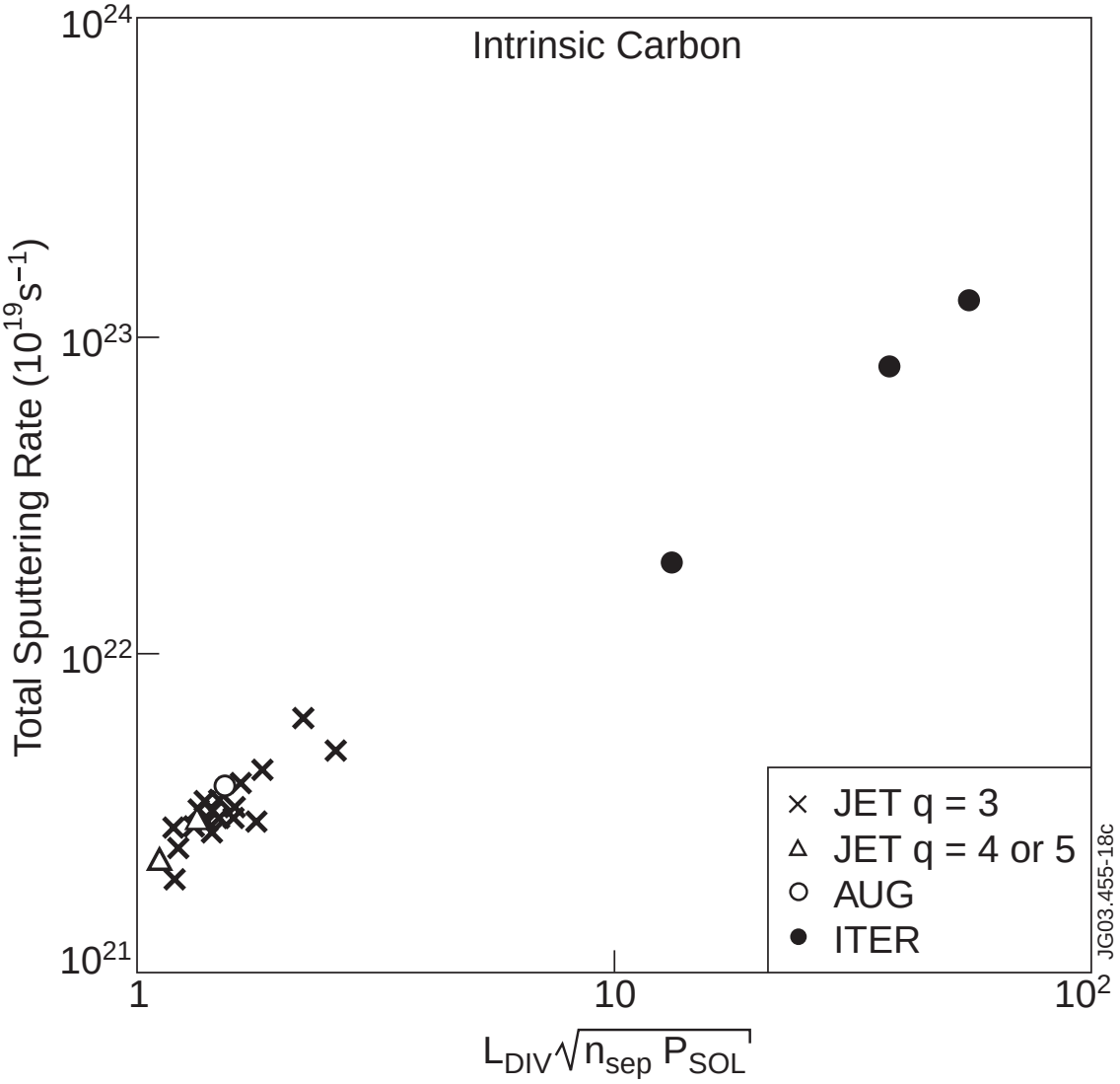
Intrinsic Carbon
Total Sputtering Rate ($10^{19}s^{-1}$)
10^{24}
10^{23}
10^{22}
10^{21}
1
10
10^2
$L_{DIV}\sqrt{n_{sep}\ P_{SOL}}$
JET q = 3
JET q = 4 or 5
AUG
ITER
JG03.455-18c

Figure 20.

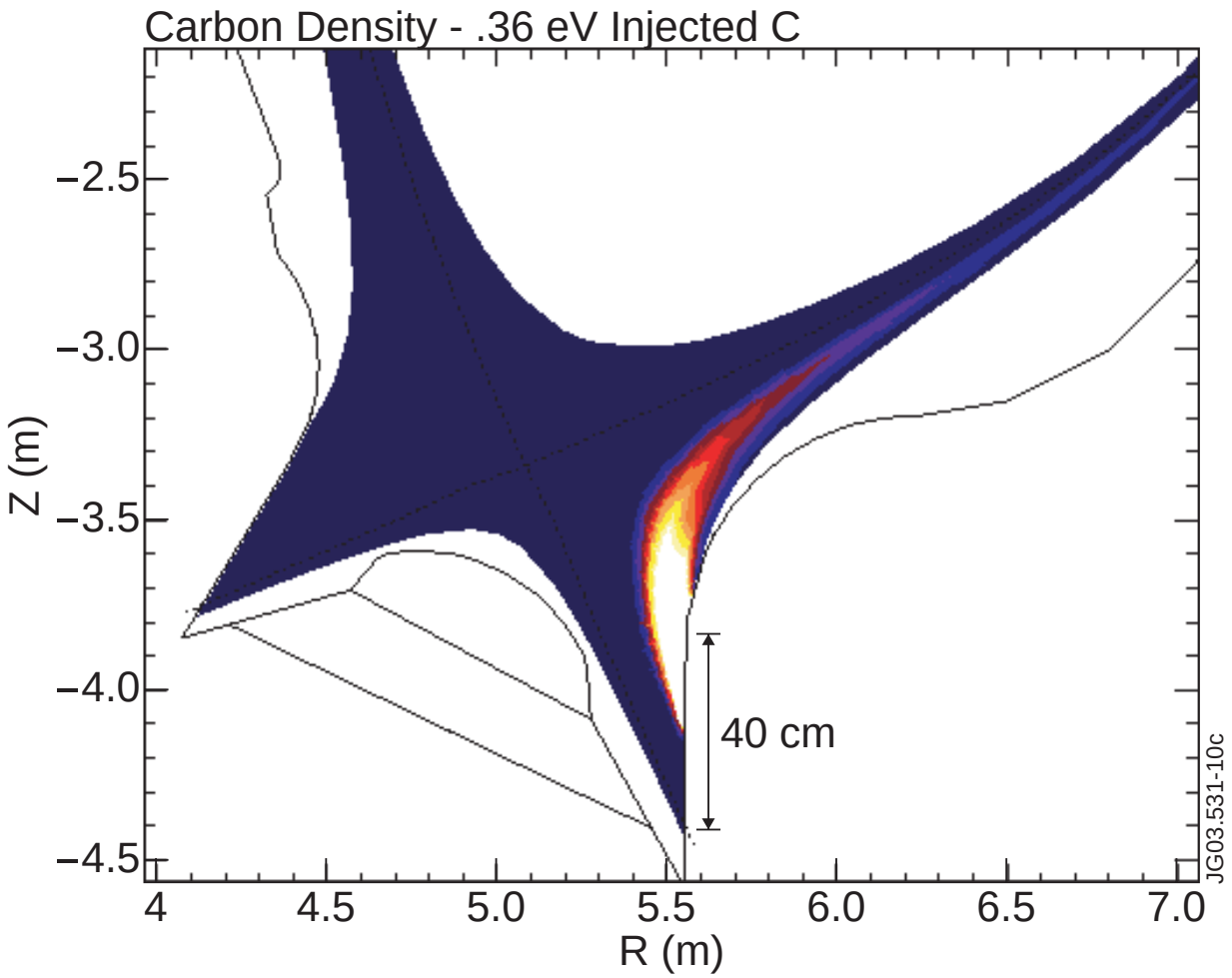
Carbon Density - .36 eV Injected C
−2.5
−3.0
−3.5
−4.0
−4.5
Z (m)
4
4.5
5.0
5.5
6.0
6.5
7.0
R (m)
40 cm
JG03.531-10c

Fig. 21

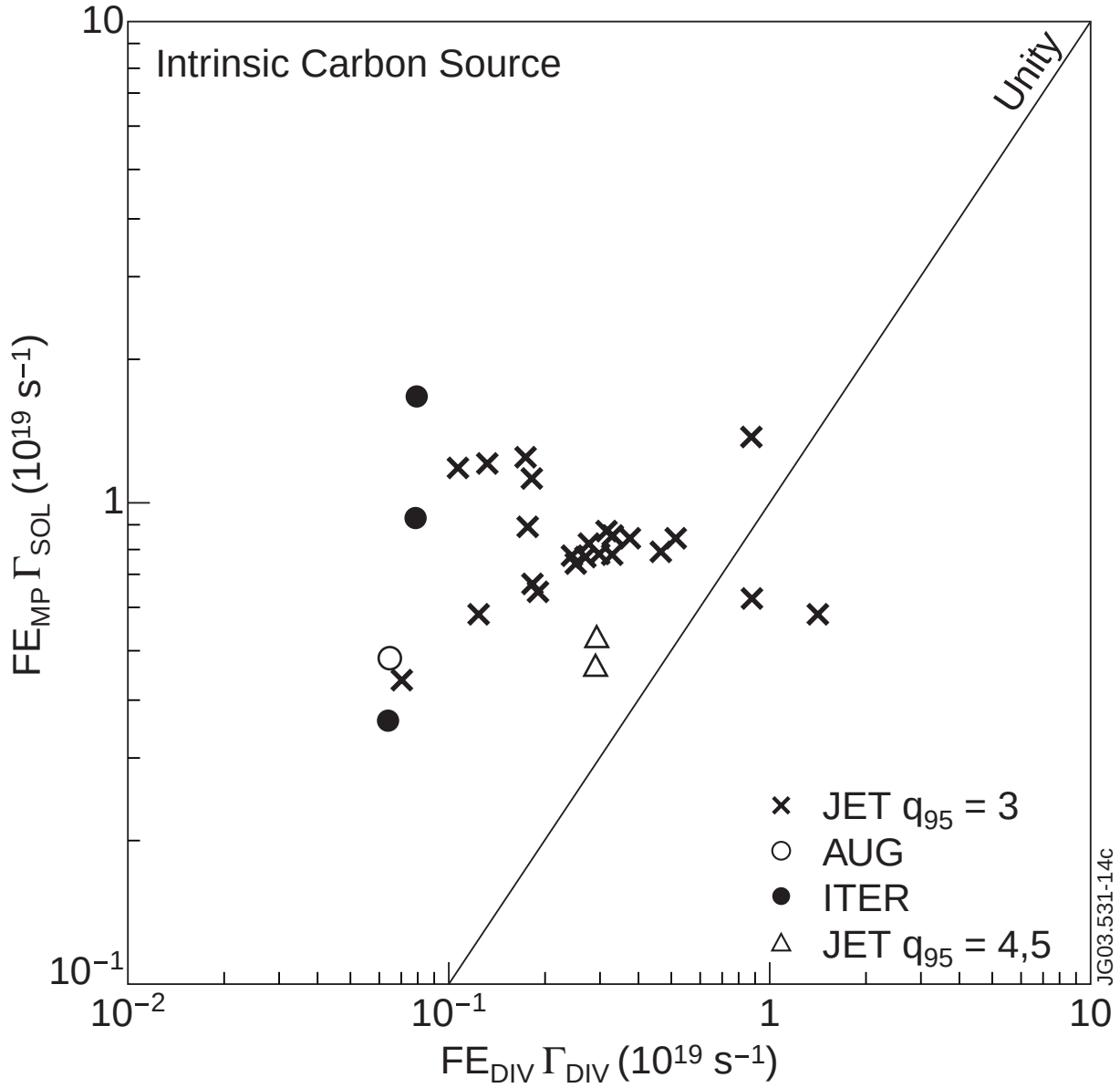
Intrinsic Carbon Source
Unity
10
1
10^{-1}
10^{-2}
10^{-1}
1
10
$FE_{MP}\,\Gamma_{SOL}\,(10^{19}\,s^{-1})$
$FE_{DIV}\,\Gamma_{DIV}\,(10^{19}\,s^{-1})$
JET q_{95} = 3
AUG
ITER
JET q_{95} = 4,5
JG03.531-14c

Figure 22

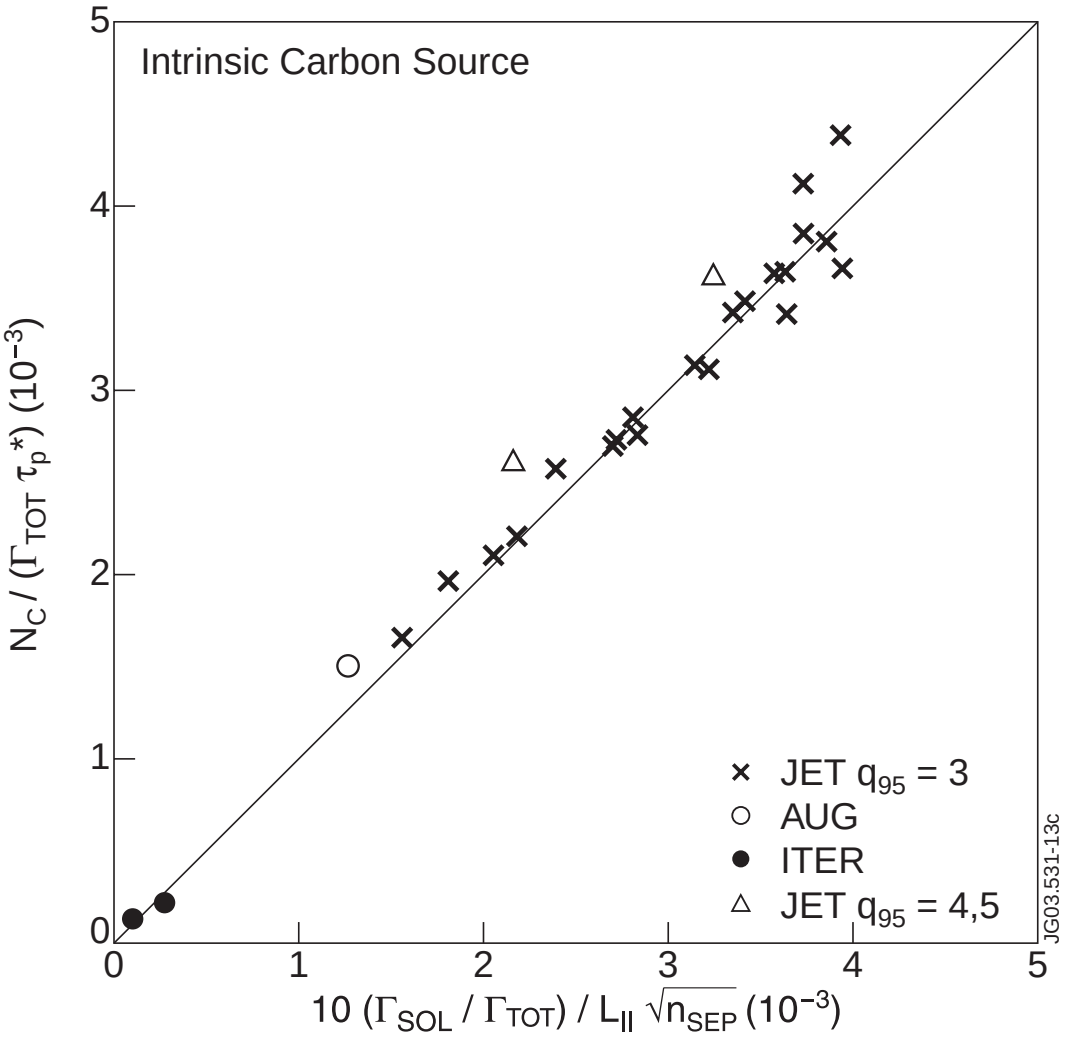
Intrinsic Carbon Source
$N_C / (\Gamma_{TOT}\ \tau_p^*)\ (10^{-3})$
$10\ (\Gamma_{SOL} / \Gamma_{TOT}) / L_{II}\ \sqrt{n_{SEP}}\ (10^{-3})$
JET q_{95} = 3
AUG
ITER
JET q_{95} = 4,5
JG03.531-13c
0
1
2
3
4
5

Figure 23

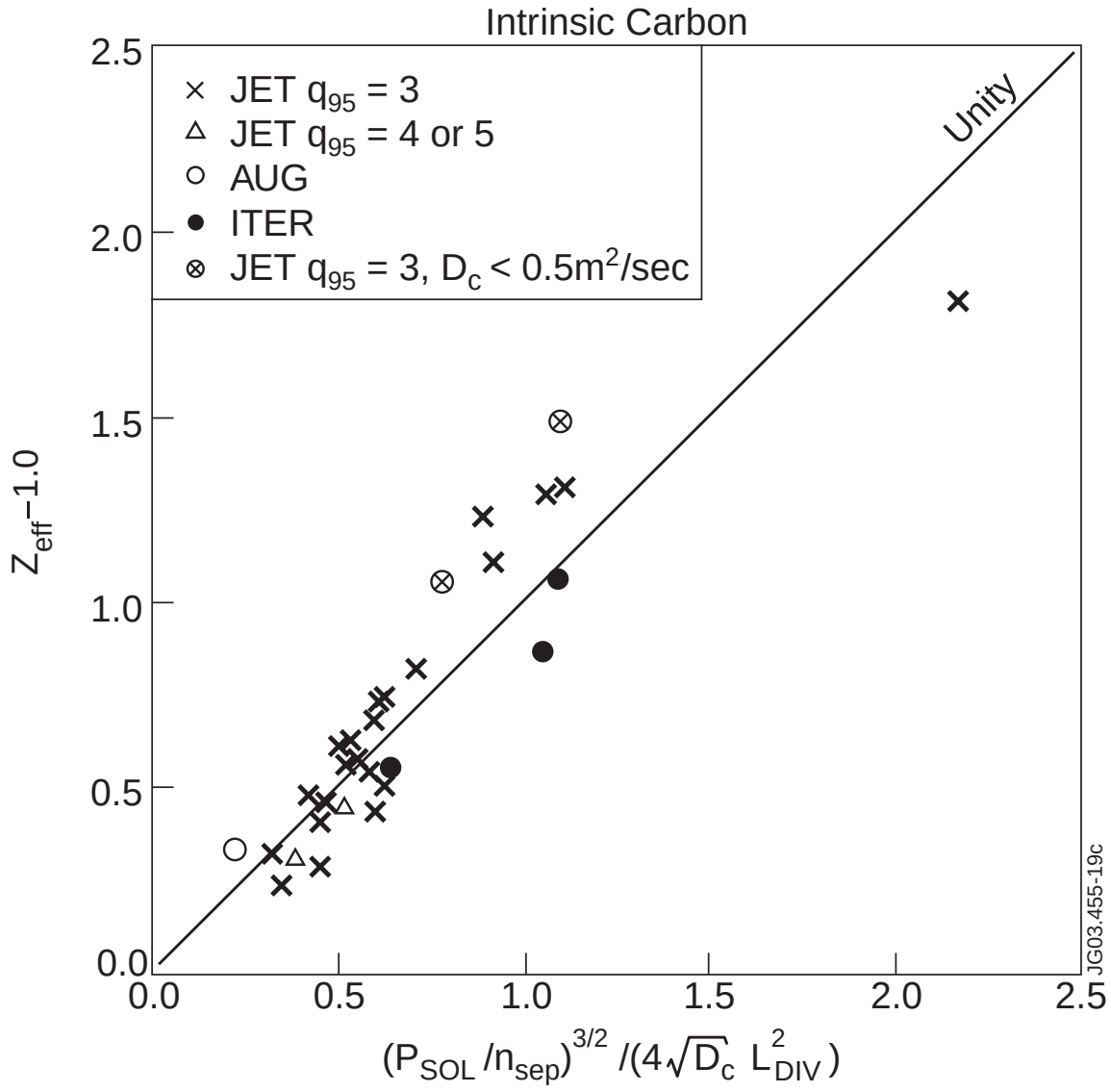
Intrinsic Carbon
JET q_{95} = 3
JET q_{95} = 4 or 5
AUG
ITER
JET q_{95} = 3, D_c < 0.5m^2/sec
Unity
Z_{eff}−1.0
$(P_{SOL}/n_{sep})^{3/2}/(4\sqrt{D_c}\ L_{DIV}^2)$
0.0
0.5
1.0
1.5
2.0
2.5
JG03.455-19c

Figure 24.

External Distribution

Plasma Research Laboratory, Australian National University, Australia

Professor I.R. Jones, Flinders University, Australia

Professor João Canalle, Instituto de Fisica DEQ/IF - UERJ, Brazil

Mr. Gerson O. Ludwig, Instituto Nacional de Pesquisas, Brazil

Dr. P.H. Sakanaka, Instituto Fisica, Brazil

The Librarian, Culham Laboratory, England

Mrs. S.A. Hutchinson, JET Library, England

Professor M.N. Bussac, Ecole Polytechnique, France

Librarian, Max-Planck-Institut für Plasmaphysik, Germany

Jolan Moldvai, Reports Library, Hungarian Academy of Sciences, Central Research Institute for Physics, Hungary

Dr. P. Kaw, Institute for Plasma Research, India

Ms. P.J. Pathak, Librarian, Institute for Plasma Research, India

Ms. Clelia De Palo, Associazione EURATOM-ENEA, Italy

Dr. G. Grosso, Instituto di Fisica del Plasma, Italy

Librarian, Naka Fusion Research Establishment, JAERI, Japan

Library, Laboratory for Complex Energy Processes, Institute for Advanced Study, Kyoto University, Japan

Research Information Center, National Institute for Fusion Science, Japan

Dr. O. Mitarai, Kyushu Tokai University, Japan

Dr. Jiangang Li, Institute of Plasma Physics, Chinese Academy of Sciences, People's Republic of China

Professor Yuping Huo, School of Physical Science and Technology, People's Republic of China

Library, Academia Sinica, Institute of Plasma Physics, People's Republic of China

Librarian, Institute of Physics, Chinese Academy of Sciences, People's Republic of China

Dr. S. Mirnov, TRINITI, Troitsk, Russian Federation, Russia

Dr. V.S. Strelkov, Kurchatov Institute, Russian Federation, Russia

Professor Peter Lukac, Katedra Fyziky Plazmy MFF UK, Mlynska dolina F-2, Komenskeho Univerzita, SK-842 15 Bratislava, Slovakia

Dr. G.S. Lee, Korea Basic Science Institute, South Korea

Institute for Plasma Research, University of Maryland, USA

Librarian, Fusion Energy Division, Oak Ridge National Laboratory, USA

Librarian, Institute of Fusion Studies, University of Texas, USA

Librarian, Magnetic Fusion Program, Lawrence Livermore National Laboratory, USA

Library, General Atomics, USA

Plasma Physics Group, Fusion Energy Research Program, University of California at San Diego, USA

Plasma Physics Library, Columbia University, USA

Alkesh Punjabi, Center for Fusion Research and Training, Hampton University, USA

Dr. W.M. Stacey, Fusion Research Center, Georgia Institute of Technology, USA

Dr. John Willis, U.S. Department of Energy, Office of Fusion Energy Sciences, USA

Mr. Paul H. Wright, Indianapolis, Indiana, USA

The Princeton Plasma Physics Laboratory is operated
by Princeton University under contract
with the U.S. Department of Energy.

Information Services
Princeton Plasma Physics Laboratory
P.O. Box 451
Princeton, NJ 08543

Phone: 609-243-2750
Fax: 609-243-2751
e-mail: pppl_info@pppl.gov
Internet Address: http://www.pppl.gov